Summer 2013

Liquid phase sintering of $20Bi(Zn_{0.5}Ti_{0.5})O_3$-$80BaTiO_3$ dielectrics with bismuth-zinc-borate and bismuth borosilicate glasses

David I. Shahin

Department:

LIQUID PHASE SINTERING OF $20Bi(Zn_{0.5}Ti_{0.5})O_3$-$80BaTiO_3$ DIELECTRICS WITH BISMUTH-ZINC-BORATE AND BISMUTH BOROSILICATE GLASSES

By

DAVID I. SHAHIN

A Thesis

Presented to the Faculty of the Graduate School of

MISSOURI UNIVERSITY OF SCIENCE AND TECHNOLOGY

In Partial Fulfillment of the Requirements for the Degree of

MASTER OF SCIENCE

in

CERAMIC ENGINEERING

2013

Approved by:

Wayne Huebner, Advisor

Geoff Brennecka

Richard Brow

ABSTRACT

Dielectrics in the $Bi(Zn_{0.5}Ti_{0.5})O_3$-$BaTiO_3$ system (specifically 20BZT-80BT, in mol%) are promising candidates for high energy density capacitor applications due to broad temperature-dependent dielectric constant maxima and a relatively field-independent permittivity. Bulk samples require sintering temperatures ≥1180°C to reach useful densities. Due to incompatibility of Bi with low-pO_2 processing, BZT-BT-based multilayer capacitors must utilize noble metal electrodes that resist oxidation during sintering. Sintering temperatures must be reduced to allow use of less expensive electrode materials (Cu, etc.). This work studies the reduced temperature sintering behavior and dielectric properties of BZT-BT sintered with $30Bi_2O_3$-$30ZnO$-$40B_2O_3$ and $50Bi_2O_3$-$25B_2O_3$-$25SiO_2$ (mol%) liquid phase formers.

Dielectrics sintered with 1v% borate additions and 5v% additions of either the borate or borosilicate achieved relative densities ≥95% after sintering at 1000°C for four hours. All compositions retained the relaxor behavior exhibited by pure 20BZT-80BT. Increased borate additions led to greater dielectric constant reductions, while increased borosilicate additions yielded no clear trend in the dielectric constant reduction. Energy densities were estimated between 0.3-0.5 J/cm^3; smaller glass additions typically led to larger energy densities. Dielectrics sintered with 1v% borate additions are of interest due to their high relative densities (≈96%) and energy densities of ≈0.5 J/cm^3 under 100kV/cm electric fields.

Studies of BZT-BT/glass interfaces revealed the formation of crystalline interfacial layers ≤10μm thick. The borate formed a bismuth titanate phase (likely $Bi_4Ti_3O_{12}$) during heating to 700°C, whereas the borosilicate formed a barium silicate phase (likely $BaSiO_3$) during processing to 800°C. Similar phases are expected to be present in the liquid phase sintered dielectrics and likely affect the BZT-BT sintering and dielectric behavior.

ACKNOWLEDGEMENTS

I owe a great deal to the many people who assisted and supported me as I performed the research presented in this thesis. First, I would like to thank my advisors, Drs. Wayne Huebner and Geoff Brennecka, for taking me as their student and for all of their guidance and encouragement during this project. I also thank Dr. Richard Brow for his advice as a member of my committee.

I also wish to thank my former colleagues at Sandia National Laboratories who became my mentors and friends during the course of my research. In particular, I owe Drs. Jon Ihlefeld, Harlan Brown-Shaklee, Mandy Brennecka, Nelson Bell, and Dara Gough, along with Mia Blea, Jill Wheeler, Bonnie McKenzie, and Sandra Jiron for their knowledge, time, and friendship.

At Missouri S&T, Dr. Mary Reidmeyer has never hesitated to take time out of her day to help me solve odd problems, find lab supplies, blow glass, and just sit down for lunch and shoot the breeze. She has taught me a great deal over the years, and has become one of my closest friends and mentors.

I also wish to thank my friends, especially Matt Halligan, Brandon and Tina Witcher, Aaron Murray, and TJ McDonough, for all of the good times, comedy, and general craziness they have shared with me.

I must thank my mother and father, and my sister Jamie. My family has always supported me with their endless love and prayers. They have always had my back and inspired me to aim for greatness. I could not have gotten to where I am without them.

Lastly, I owe a special debt of gratitude to my bride-to-be, Katie. Since we met, she has shared in all my successes, and lifted me up from all of my failures. I cannot thank her enough for all of the joy and love she has brought into my life, and for sticking with me during all of the time we had to spend apart to allow me to fulfill my academic pursuits. Her grace, patience, and love have truly been a blessing in my life.

TABLE OF CONTENTS

LIST OF ILLUSTRATIONS

Page

LIST OF TABLES

Page

1. INTRODUCTION

The research presented in this thesis was performed to improve the suitability of $Bi(Zn_{0.5}Ti_{0.5})O_3$-$BaTiO_3$ (BZT-BT) ceramic dielectrics for high energy density capacitor applications. Compositions in the BZT-BT binary system (specifically for BZT concentrations around 20 mol%) have been shown to exhibit relaxor ferroelectric behavior. Relaxor behavior is characterized by a broad, frequency-dependent maximum in dielectric constant as a function of temperature, and by narrow/closed hysteresis in field-dependent polarization. In the 20 mol% BZT-80 mol% BT system specifically, the dielectric constant remains high (≈2000) on heating from the temperature of maximum dielectric constant, T_m, to 175°C. T_m ranges from 30°C (at a measurement frequency of 100Hz) to 100°C (at 100kHz), giving a broad range of operating temperatures for capacitors utilizing these dielectrics. The dielectric constant for this system is also relatively field-independent for electric fields as high as 100kV/cm; this allows for storage of large quantities of energy at high field strengths, while narrow polarization-field loops indicate minimal dielectric loss. These dielectrics are thus promising candidates for high field and high energy density capacitor applications.[1]

The specific focus of this research was to reduce the processing temperatures associated with BZT-BT dielectrics for purposes of cost reduction and mass production. To survive electric fields ≥100kV/cm, the dielectric must be sintered to high densities (95-100% of theoretical). Pure BZT-BT dielectrics must be sintered at 1180°C for 12 hours to reach suitable densities.[1] Electrodes in multilayer ceramic capacitors must be co-fired with the dielectric; to survive the BZT-BT sintering temperatures and high pO_2 levels required for Bi processing, electrodes must be comprised of expensive noble metals (Ag/Pd or Pt). Use of cheaper electrode materials (Ni, Cu, etc.) requires a reduction in sintering temperature, which in turn requires the addition of other materials into the ceramic to aid in sintering at reduced temperatures. This work represents a first

attempt at selection and incorporation of sintering aids into BZT-BT dielectrics. A primer on the important concepts that shaped the direction of this research and a review of current literature is given in Section 2. Basic characterization of the selected sintering aids ($30Bi_2O_3$-30ZnO-$40B_2O_3$ and $35Bi_2O_3$-30ZnO-$35B_2O_3$, in mol%) and their interactions with the BZT-BT is described in Section 3. Section 4 describes the microstructural evolution observed in the BZT-BT with 5 vol% additions of the sintering aids, and Section 5 reports the effects of 1, 2, and 5 vol% additions of each sintering aid on the dielectric properties of the BZT-BT. Conclusions and recommendations for additional characterization/analyses are given in Section 6. The Appendix reports additional work on a third sintering aid composition, $35Bi_2O_3$-30ZnO-$35B_2O_3$.

2. RESEARCH BACKGROUND

This section provides basic explanations of the electrical/material properties and processes fundamental to this research. A brief introduction to capacitor terminology and operation, ferroelectricity, and relaxor ferroelectricity is given in order to indicate the principle properties important for high energy density and high power density capacitors. A current literature review describes the key beneficial properties and processing difficulties associated with the BZT-BT dielectric system for these applications. Liquid phase sintering is presented as a potential solution to these difficulties, and the important criteria in selecting liquid phase additives are explained in the context of this research.

2.1. CAPACITOR FUNDAMENTALS

Capacitors are common electronic devices capable of storing electrical energy through charge buildup from the application of an electric field. In a capacitor (shown schematically in FIG. 2-1), two conductive electrodes are physically separated. The application of an external voltage across the capacitor creates an electric field (E) between the electrodes, which induces charge buildup at the electrode surfaces. Charge storage can be increased by insertion of a dielectric medium that prevents charge conduction between the electrodes and that may also polarize in response to the external electric field.

In the case of ceramic dielectrics, ions in the dielectric crystal lattice can shift slightly around their lattice sites in response to the field. Ionic shifting creates an internal electric field in the dielectric that opposes the external field. As a result, the net field across the dielectric is reduced; this allows application of a stronger external field and more energy to be stored in the capacitor.

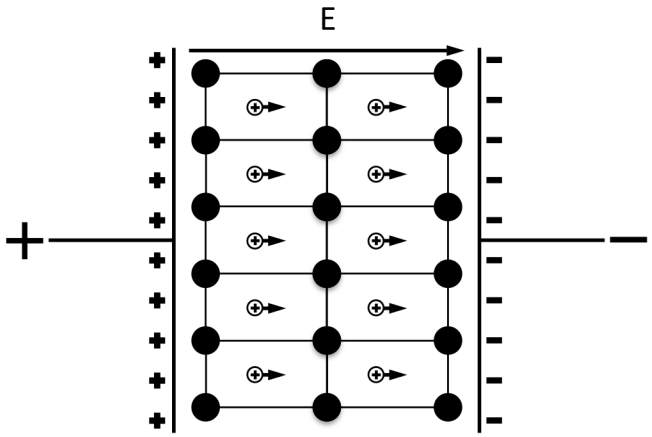

FIG. 2-1. Capacitor schematic showing charge buildup on electrodes, electric field direction within the capacitor, and the corresponding positional shifting of ions in the dielectric.

Capacitors store charge only if an external voltage is being applied, or if the capacitor is electrically isolated. When the external voltage is first applied to the capacitor, charge buildup on the electrodes occurs rapidly. As the increasing charge on each electrode repels incoming charges, buildup slows and eventually halts as the electric field cannot drive more charges to the electrodes. On discharge, the opposite sequence occurs; initially the discharge current from the capacitor is high, and decreases over time as the capacitor charge decreases.

2.2. CAPACITOR PROPERTIES AND EQUATIONS

Capacitance (C, Farads) measures of the amount of charge stored by a capacitor at a given applied voltage. For a parallel-electrode capacitor geometry,

$$C = \frac{Q}{V} = \frac{\varepsilon_0 K A}{d} \tag{2-1}$$

where:

Q = Charge stored in the capacitor (Coulombs)

V = External voltage applied to the capacitor (Volts)

ε_0 = Permittivity of free space (8.854E-12 F/m)

K = Dielectric constant/relative permittivity of the dielectric, also denoted as ε_r

A = Electrode surface area (m^2)

d = Electrode separation distance (m).

The dielectric constant is defined as the ratio of the capacitance of a capacitor with a dielectric to the capacitance of a dielectric-free capacitor, and, in turn, the ratio of the (real) portion of permittivity to the vacuum permittivity,

$$K = \frac{C}{C_0} = \frac{\varepsilon'}{\varepsilon_0} \tag{2-2}$$

where:

C_0 = Capacitance of an identical capacitor without the dielectric (Farads)

ε' = Real portion of the relative permittivity

The dielectric permittivity is a complex quantity, made up of a real (ε') component and an imaginary (ε'') component. Capacitors in alternating current (AC) and direct current (DC) circuits are modeled as a capacitor in series with a resistor whose resistance value is the equivalent series resistance, or ESR. For an idealized capacitor, no current conducts or "leaks" through the dielectric; the ESR is infinite, such that the current and voltage are 90° out of phase. In an actual capacitor, however, some current leakage occurs, and the ESR is finite. This causes the current and voltage to be shifted to less than 90° out of phase by some angle δ. The leakage current represents dielectric loss, represented by ε", while the real portion of the permittivity, ε', reflects the capacitive portion of the dielectric constant. The loss angle δ relates ε' and ε". The dissipation factor, or loss tangent, is represented by

$$Loss\ Tangent = \tan\delta = \frac{\varepsilon''}{\varepsilon'} \tag{2-3}$$

where:

ε” = Dielectric loss (imaginary/resistive component of relative permittivity)

Energy density (energy stored per unit volume) is a quantity of particular importance for energy storage and power regulation systems. The energy density E_d (J/m^3) of a capacitor is given by

$$E_d = \frac{1}{2}\varepsilon_0 K E^2 \qquad (2\text{-}4)$$

where:

E = Applied electric field (V/m)

The applied field E is thus an important quantity for capacitors intended for energy storage, as energy density varies directly with E^2. The dielectric constant is also important in determining the energy storage capabilities of a capacitor.

2.3. CAPACITOR TYPES AND COMPARISONS

Different varieties of capacitor exist, each with differing discharge rate capabilities (power density) and energy storage capabilities (energy density) per unit volume. FIG. 2-2 compares different capacitor types and other energy storage technologies, such as batteries, in terms of energy and power density. Ceramic capacitors rely on formation of electric dipoles caused by ions shifting away from their equilibrium (zero-field) lattice sites for charge storage. This dipole polarization occurs rapidly, and as such, ceramic capacitors have comparatively high charge/discharge rates. They cannot, however, store much charge compared to other capacitor types or batteries.

Electrolytic capacitors use a metal foil (or foam) and a conductive liquid electrolyte as electrodes, separated by an oxide dielectric film on the metal. This thin film dielectric (≈100nm

thick) yields high capacitance and energy density, at the expense of power density due to slow charge conduction through the electrolyte.

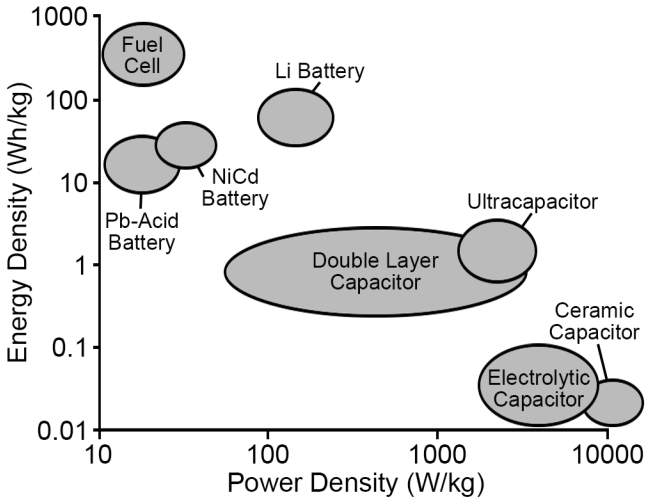

FIG. 2-2. Ragone plot showing energy and power densities of various energy systems. (Chart data from Abdullah.[2])

Super- and ultracapacitors (both double-layer capacitors) utilize high surface area materials (typically porous carbon) and a liquid electrolyte to form an electrical double layer of ions that acts as a dielectric. The small thickness (1-2 ions, 0.5-1.0 nm thick) of the double layer and the high surface area of the solid electrode allow supercapacitors to attain the greatest energy density values of any capacitor type. Supercapacitors also exhibit the lowest power densities of all capacitor varieties due to the large distance charge must travel to exit the capacitor.[3]

Batteries, by comparison, have a much larger energy density than all capacitors, but have a much smaller power density due to the relatively slow chemical reactions utilized to generate current.

The high power density of capacitors relative to other technologies makes them useful for power stabilization applications. During a power failure in any electrical system, from a small

circuit to a national electric grid, capacitors can readily provide energy in the initial phases of the outage while batteries, generators, and other generation mechanisms initialize and begin providing energy. Ceramic capacitors, with their high power densities, would be ideally suited to power stabilization immediately after system failure. A major limitation of ceramic capacitors lies in their energy density capabilities; energy densities must be improved in order for such capacitors to be potentially useful as stabilization devices. Development of novel ceramic dielectrics capable of storing large amounts of energy at high electric field strengths will increase the energy density (and thus utility) of ceramic capacitors.

2.4. FERROELECTRICITY IN CERAMICS

Most ceramics are classified as paraelectrics – materials that are polarized only in the presence of an electric field. Upon removal of the field, polarization in a paraelectric returns to zero. Ferroelectric materials, however, retain some polarization after removal of the electric field. The defining feature of a ferroelectric is this spontaneous or remanent polarization under zero-field conditions (P_r); furthermore, the remanent polarization can be reversed by application of electric fields in the opposite direction of the polarization.

Ferroelectricity originates from the existence of polarization axes within specific crystal structures that allow polarization without an applied field. These crystal structures must be non-centrosymmetric and have multiple stable sites along the polarization axes that ions can occupy. Electric fields can move these ions from one stable location to another along the axis, thereby polarizing the crystal unit cells.

Of the 32 crystal classes, only ten exhibit polarization axes suitable for spontaneous polarizations, and only several of the ten have the reversible polarization of a ferroelectric.[4] Many common ferroelectrics, such as $BaTiO_3$ and $Pb(Zr,Ti)O_3$, fall into one of the ferroelectric structures, known as the perovskites (ABO_3). In these structures, such as the tetragonal $BaTiO_3$

unit cell shown in FIG. 2-3, the B-site cation(s) lie within a distorted oxygen octahedron. The distortion allows the Ti^{4+} ion to shift off-center along the [001] axis of the unit cell.

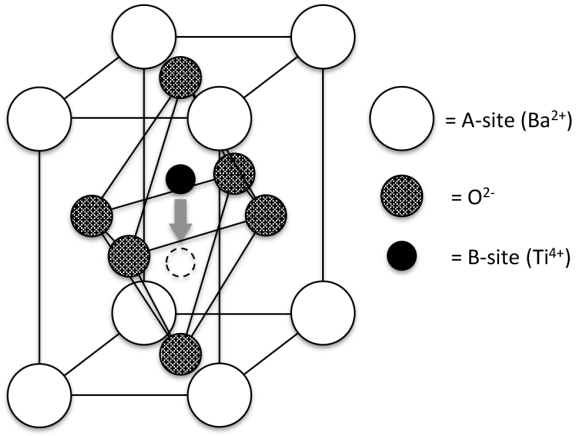

FIG. 2-3. Tetragonal ABO_3 structure of many ferroelectric ceramics; the B-site cation can polarize along the c-axis within the distorted oxygen octahedron.

On heating, ferroelectric crystals typically undergo a phase transition from a ferroelectric to a higher symmetry paraelectric structure. The temperature at which this phase transition occurs is known as the Curie temperature (T_c). The transition is accompanied by a spike in dielectric constant, due to structural instability between the ferroelectric and paraelectric phases near T_c. A typical K versus temperature plot for single crystal $BaTiO_3$, shown in FIG. 2-4, illustrates the sharp permittivity increase at the Curie temperature of ≈120°C. Polycrystalline ferroelectrics exhibit broader permittivity peaks at T_c that are grain size-dependent.[5]

Ferroelectrics exhibit hysteretic behavior in polarization when measured as a function of electric field. Adjacent crystalline unit cells in a ferroelectric will polarize in the same direction, forming larger regions, known as domains, with a net polarization.

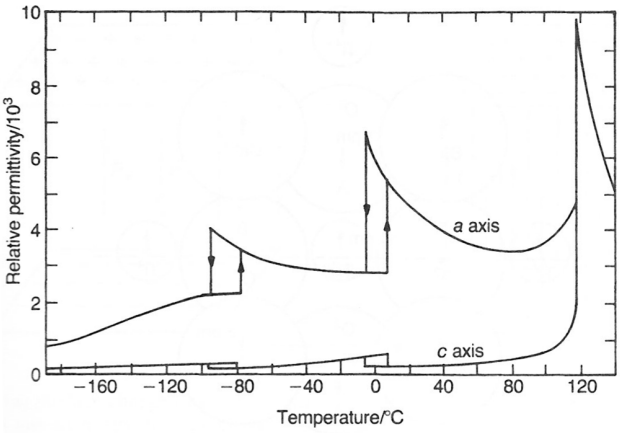

FIG. 2-4. Dielectric constant vs. temperature plot for single crystal $BaTiO_3$, as measured in the a- and c-directions.[3]

Prior to application of an external electric field, the polarization directions of the ferroelectric domains are set by the crystalline symmetry and orientation of individual grains. For a sintered ferroelectric with ∞∞m symmetry, the bulk ceramic has a zero net polarization. With application of a field, domain walls separating differently oriented domains shift to align polarization vectors with the field to create a non-zero net polarization in the bulk. As the field strength increases, the ferroelectric will continue to polarize until reaching saturation, above which field strength increases cease to cause further dipolar polarization. Saturation is represented by the linear section at each end of the polarization-field loop. Decreasing the field decreases the polarization in the ferroelectric, as some domains reorient to minimize the internal energy of the crystal. Some of the domains will remain polarized in the direction of the field, such that, under zero-field conditions, the ferroelectric retains a net remanent polarization (P_r). Reversing the field will cause the polarization to begin to reverse as the domain polarizations shift towards the opposite direction. Once the coercive field (E_c) value has been reached, the net polarization becomes zero, and then increases in the opposite direction. This gives rise to a dielectric hysteresis loop, shown in FIG. 2-5 for a single crystal and polycrystalline ceramic. The single crystal exhibits a “square loop”; on reaching the coercive field value, (nearly) all domains

switch direction at once. Polycrystals exhibit slanted loops, as the domains do not switch direction to match the field change as rapidly.

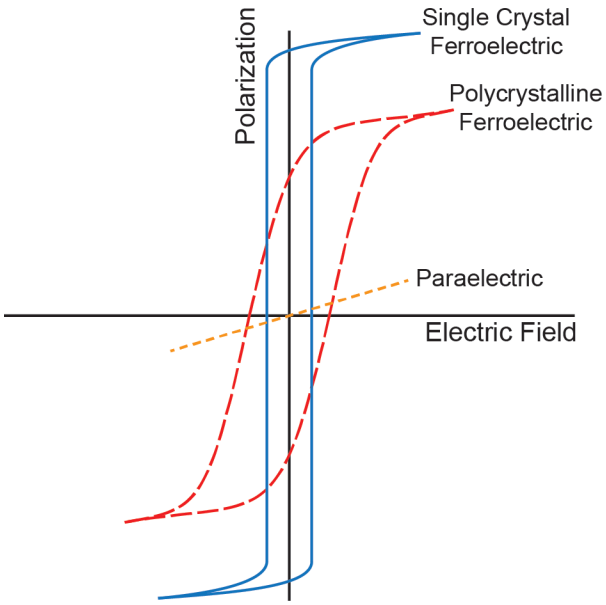

FIG. 2-5. Generalized polarization-electric field plot showing hysteresis and reversible remanent polarizations typical of ferroelectrics and the linear behavior of paralectrics.

2.5. RELAXOR FERROELECTRICS

Relaxor ferroelectrics (relaxors) are a special class of ferroelectrics that behave quite differently from "normal" ferroelectrics. Relaxor behavior, shown in FIG. 2-6, is characterized by a diffuse maximum in the temperature-dependent dielectric constant, and by dispersion in the dielectric constant as a function of measurement frequency.

Relaxor behavior occurs in ceramic systems with several aliovalent cations substituted onto the A- and/or B-sites.[6] Random cation substitution creates local electric dipoles within individual unit cells. Unit cells adjacent to these dipoles polarize within a very small radius

(known as the correlation length), leading to the formation of nanodomains in the relaxor. Because nanodomain polarization is induced by lattice disorder, rather than structural distortion as in normal ferroelectrics, complex cubic perovskites can exhibit relaxor behavior.

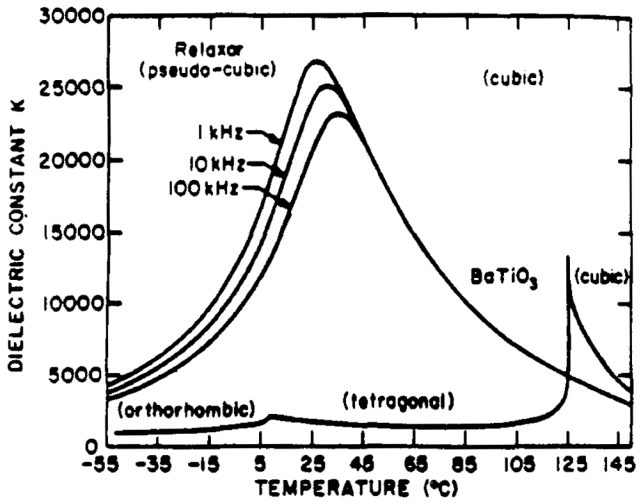

FIG. 2-6. Comparison of temperature-dependent dielectric constant behavior for a relaxor ferroelectric ($0.93Pb(Mg_{1/3}Nb_{2/3})O_3$-$0.07PbTiO_3$) and a normal ferroelectric ($BaTiO_3$).[7]

The electrical behavior of relaxor systems departs tremendously from the behavior of traditional ferroelectrics. At the temperature corresponding to the maximum dielectric constant (T_m), no structural transition occurs, as is the case when normal ferroelectrics pass through the Curie temperature. Since no structural change takes place, nanodomains persist above T_m up to the Burns temperature (T_d), and the dielectric constant decreases smoothly from the maximum at T_m. Frequency dispersion in the temperature-dependent dielectric constant arises from the large number of equivalent polarization directions in cubic lattices.[4]

Electric field-dependent polarization behavior also differs between relaxors and normal ferroelectrics, as shown in FIG. 2-7. Instead of the "open" hysteresis loops seen in normal ferroelectrics, relaxors exhibit closed or "slim" loops with a near-zero remanent polarization

(FIG. 2-7a). These slim loops result from the nanodomains returning to a random orientation following removal of the electric field.[8]

The dielectric constant, energy storage, and energy loss can be determined from the P-E loops. The dielectric constant can be found at specific electric field strengths as the local slope of the loop. Energy stored in the dielectric can be found from the area captured between the P-E loop and the polarization axis. Energy loss can be measured from the area contained by the loop. Some relaxor systems maintain high dielectric constants under high field strengths and can store larger amounts of energy, relative to normal ferroelectrics and paraelectrics, with minimal loss (as indicated in FIG. 2-7b). This P-E behavior, combined with high dielectric constant values over a wide range of temperatures, makes these relaxor systems ideally suited for high energy density ceramic capacitor dielectrics.

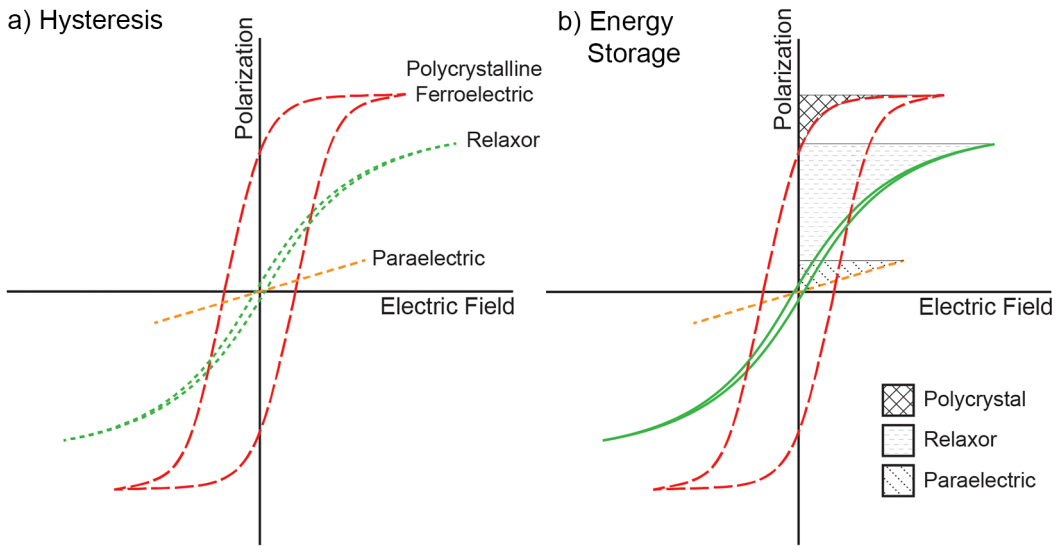

FIG. 2-7. Polarization-electric field and energy storage behavior of a relaxor ferroelectric, polycrystalline normal ferroelectric, and paraelectric material.

2.6. CURRENT RESEARCH REVIEW

Many common relaxor compositions are based on Pb-containing solid solutions such as PMN ($Pb(Mg_{1/3}Nb_{2/3})O_3$) or PLZT ($(Pb,La)(Zr_{1-x}Ti_x)O_3$). Despite having useful dielectric properties, including high dielectric constants, pyroelectric coefficients, and piezoelectric coefficients, Pb-based dielectrics are also hazardous substances.[6, 8] This classification created the need for environmentally-benign substitutes that still possess useful dielectric characteristics, particularly at high electric fields for energy storage applications. Current research has focused on bismuth-based replacements. Bismuth is a large, highly polarizable ion electronically similar to Pb, while possessing fewer health hazards.

Bismuth-based perovskite ceramics such as $Bi(Zn,Ti)O_3$ (BZT), $BiScO_3$ (BS), and $BiInO_3$ (BI) have been of particular interest.[9, 10, 11] Many of these compounds unfortunately cannot be formed under ambient pressure conditions. Creation of single-phase perovskites requires the use of hot pressing; attempts at synthesis under ambient pressures create mixtures of the end-member phases comprising each perovskite.

Incorporating the Bi-perovskites into a solid solution with another stable perovskite (such as $PbTiO_3$ or $BaTiO_3$) has allowed creation of stable ferroelectrics with altered properties relative to the parent ferroelectric.[12] Current research has focused on using Pb-free perovskites as stabilizers. $BaTiO_3$ (BT) is a natural Pb-free choice, as it has good dielectric properties and is stable as a pure compound. A variety of Bi-perovskite-$BaTiO_3$ solid solutions, such as BZT-BT, BS-BT, and $Bi(Mg,Ti)O_3$-BT (BMT-BT) have been studied with promising results, particularly for dielectric applications, as relaxor behavior occurs with sufficient additions of the Bi-perovskite.[13, 14, 15, 16, 17]

Huang and Cann found that up to 33 mol% BZT can be stabilized in solid solution with BT. BZT-BT solid solutions possess a room temperature phase boundary around 10 mol% BZT. Below 10 mol% BZT concentrations, BZT-BT exhibits the tetragonal perovskite symmetry of the

host BT, and transitions to a pseudocubic perovskite structure for higher BZT additions.[18] With this pseudocubic structure comes relaxor dielectric behavior.

The strong relaxor behavior exhibited by the 20BZT-80BT composition (as shown in FIG. 2-8) is of particular interest for high energy density capacitor applications. T_m ranged from 30°C (100Hz) to 100°C (100kHz); the dielectric constant reached peak values from 1900 (100kHz) to 2100 (100Hz) at T_m and remained above 1800 between T_m and 175°C. The 20BZT-80BT composition also exhibits the expected relaxor slim P-E loop with relatively little saturation in dielectric constant for field strengths up to 90kV/cm. Dielectrics based on this composition are thus appealing for high field energy storage applications in environments subject to a broad range of temperatures (30-175°C).

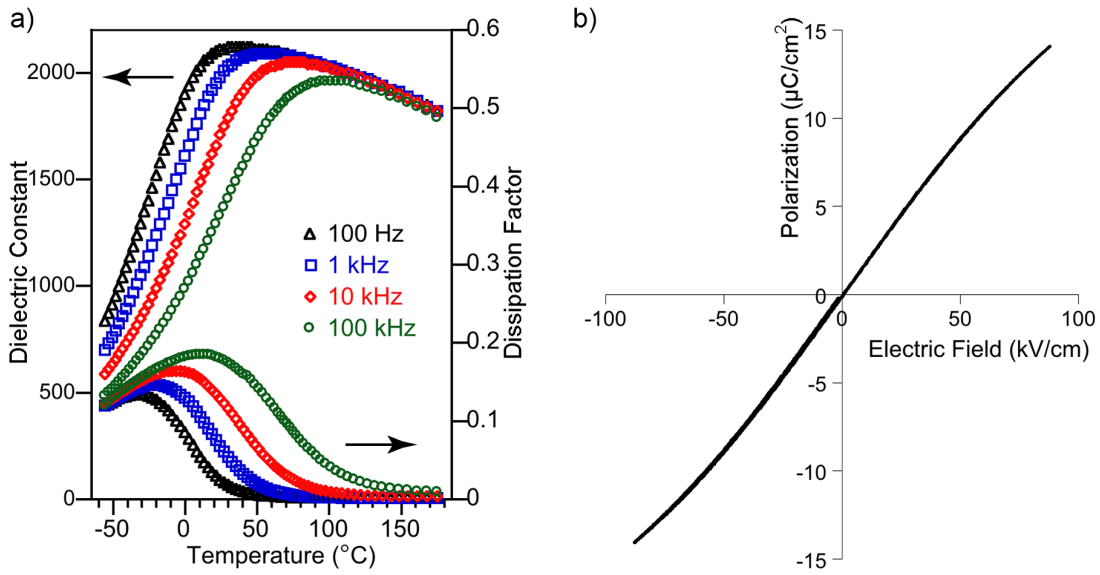

FIG. 2-8. Dielectric constant vs. temperature and polarization vs. electric field behavior for 20BZT-80BT compositions.[1]

One difficulty associated with BZT-BT and other Bi-perovskite solid solutions stems from the processing temperatures required for sintering to full density. In the case of 20BZT-80BT, the dielectric can be sintered to full density (~99% of theoretical) at 1180°C and higher.[1] Multilayer capacitors incorporating these dielectrics must utilize expensive noble metal electrodes (Pt or Ag/Pd) that do not melt at the required sintering temperatures. Electrode selection for BZT-BT multilayer capacitors is also dependent on oxygen partial pressure; the electrodes must remain reduced to a metallic state at the pO_2 conditions required to prevent reduction of the oxide dielectric during sintering at elevated temperatures.

A good approximation of viable temperature-pO_2 combinations for a complex system like BZT-BT can be made by construction of an Ellingham diagram.[19] The oxidation lines for each cation in the dielectric can be compared with the oxidation lines for candidate electrodes to determine an approximate temperature-pO_2 processing window for the combined multilayer capacitor. An Ellingham diagram showing the oxidation lines for the oxide constituents of BZT-BT and several noble and base metals (silver, nickel, and copper) is shown in FIG. 2-9. The oxidation line for $2Bi + 3/2O_2 \rightarrow Bi_2O_3$ is located at much higher pO_2 values than the lines for the other constituents of BZT-BT, indicating the likelihood of BZT-BT incompatibility with low pO_2 processing. Comparison of the location of the Bi oxidation line relative to the electrode oxidation lines indicates that Ni is an unlikely candidate for sintering with BZT-BT. Cu and Ag are possible electrode materials, provided that the BZT-BT sintering temperature can be reduced below the melting temperatures of the electrodes (1085°C for Cu, and 962°C for Ag).

Inexpensive electrode solutions such as Cu must be utilized to make BZT-BT capacitors viable for mass production. Lower cost electrodes, in turn, facilitate the need for reduced sintering temperatures. Cost reductions can also be realized from lower energy consumption with reduced sintering temperatures.

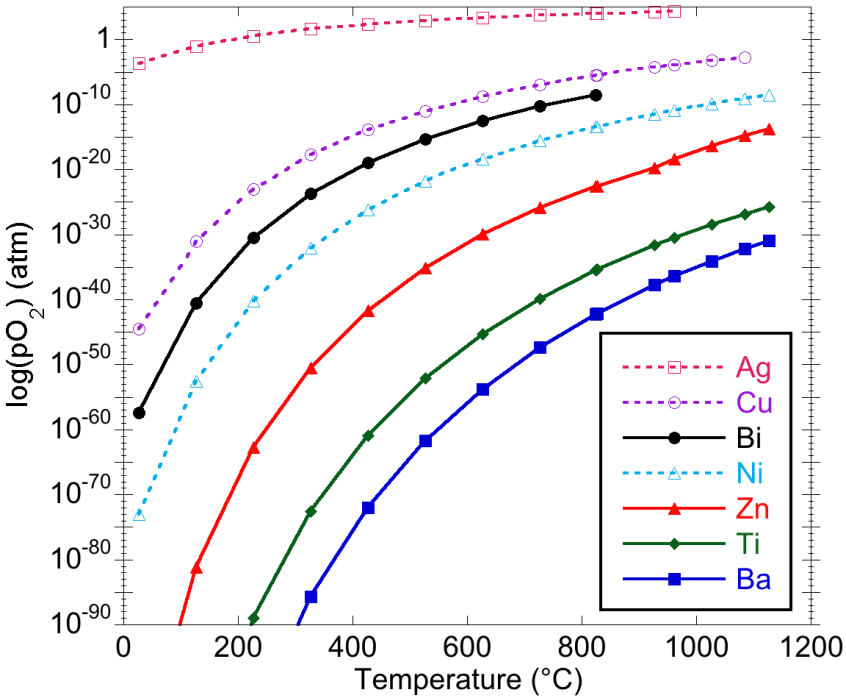

FIG. 2-9. Ellingham diagram showing oxidation lines for the oxide components of BZT-BT in relation to several electrode metals. (Data from various sources.[20, 21, 22])

2.7. LIQUID PHASE SINTERING

Liquid phase sintering presents a possible solution to the problem of reducing sintering temperatures in BZT-BT dielectrics. In this process, a second phase additive forms a liquid at temperatures lower than the solid-state sintering temperature of the bulk material. The liquid phase then assists in sintering the bulk by increasing the matter transport rate associated with desirable sintering mechanisms. This leads to densification of the bulk at lower temperatures and shorter times relative to solid-state sintering.

The key stages during liquid phase sintering are classified as follows:[23]

- *Stage 1: Particle rearrangement and liquid redistribution* – The liquid phase wets particle surfaces and fills the interstices between the particles in the low-density microstructure. Some rearrangement of the bulk phase particles also takes place as densification begins.

- *Stage 2: Solution-precipitation* – The liquid phase dissolves the solid at the liquid-particle interfaces with high chemical potentials. The dissolved material diffuses through the liquid and reprecipitates on other particle surfaces with lower chemical potentials. As a result, grains coarsen and reshape into polyhedra with flattened faces.
- *Stage 3: Final densification* – Interconnected grains trap the liquid phase into isolated pores. Grains coarsen further under solid-state diffusion conditions in regions where no liquid phase remains, while the trapped liquid assists in further densification where it exists.

These stages overlap during densification of a ceramic microstructure. The majority of densification and shrinkage occurs during Stages 1 and 2, as shown in FIG. 2-10.

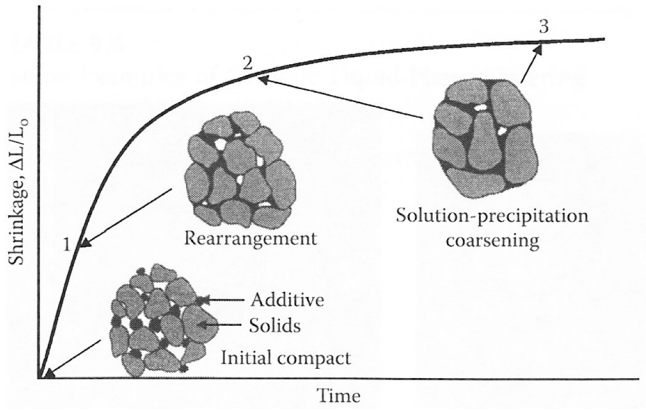

FIG. 2-10. Shrinkage behavior as a function of time for the various stages of liquid phase sintering.[23]

A number of important traits are required in an effective liquid phase sintering aid. The liquid phase should form at a low temperature relative to the bulk solid-state sintering temperature, and have a low viscosity at such temperatures. The liquid phase must also wet the bulk material (solid-liquid contact angle $\theta << 90°$) to ensure that the liquid coats the bulk grains

for uniform dissolution and precipitation. Also, the liquid phase former must be homogeneously distributed within the bulk particles to allow for uniform liquid phase sintering.

The cooling behavior of the liquid phase is of key importance to dielectric behavior. One of three behaviors is desirable on cooling of the liquid phase: recrystallization into a second phase, incorporation into the bulk phase, or retraction into the triple points along the grain boundaries to become a discontinuous phase. If the liquid phase remains continuous on cooling, the dielectric properties of the sintered material will be controlled by the continuous phase, which is likely to have a lower dielectric constant than that of the bulk ceramic, which in turn reduces the usefulness of the dielectric. The composition of any incorporated or second phases is also important, as formation of electronically or ionically conductive phases in the dielectric will increase dielectric loss through leakage currents, especially at high field strengths.

2.8. RESEARCH FOCUS

This research represents a first attempt at reducing the sintering temperature of 20BZT-80BT via additions of discreet liquid phase formers. Liquid phase sintering aids were chosen by finding glasses that were similar in composition to the BZT-BT bulk, exhibited low glass transition temperatures (T_g) and melting temperatures (T_{melt}), and had high dielectric constants. As a starting point, glasses were selected that had been effective sintering aids for pure $BaTiO_3$, due to the BZT-BT composition being comprised primarily of $BaTiO_3$. Huebner and Zhang reported success using a $50Bi_2O_3$-$25B_2O_3$-$25SiO_2$ (mol%) glass in conjunction with $BaTiO_3$; the glass properties (T_g = 370°C, T_{melt} = 645°C, K = 39.5) and composition were also in line with the initial criteria for BZT-BT liquid phase sintering aids.[24] Glasses in the Bi_2O_3-ZnO-B_2O_3 system were also selected as sintering aid candidates, due to compositional similarities, and reports of T_g values between 360-420°C and K values of 21-33 for xBi_2O_3-xZnO-$(1-2x)B_2O_3$ ($0.3 \leq x \leq 0.4$).[25]

Preliminary studies were conducted on one glass in the bismuth zinc borate system ($30Bi_2O_3$-$30ZnO$-$40B_2O_3$, mol%) and one in the bismuth borosilicate system ($50Bi_2O_3$-$25B_2O_3$-$25SiO_2$, mol%). Thermal analyses, wetting angle studies, and dielectric measurements were performed on these glasses as screening studies to determine the viability of these glasses as sintering aids for 20BZT-80BT. Density and microstructural evaluations were then performed on 20BZT-80BT sintered with additions of 1, 2, and 5v% of each glass to determine any improvements in sintering and densification (i.e. reduced sintering temperatures) imparted by additions of the glasses. Dielectric characterization was performed on parts that reached a relative bulk density of >89% after sintering, to determine the effects of glass additions on the dielectric properties of the 20BZT-80BT.

3. PRELIMINARY STUDIES

The $30Bi_2O_3$-30ZnO-$40B_2O_3$ and $50Bi_2O_3$-$25B_2O_3$-$25SiO_2$ glasses were subjected to a series of initial analyses to characterize their bulk thermal and dielectric properties, as well as their interactions with 20BZT-80BT powders during sintering. The results of these studies as reported in this section were used to determine the viability of each glass as liquid phase sintering aids for BZT-BT.

3.1. DIELECTRIC AND GLASS FORMULATION

Dielectric powders comprised of 20mol% $Bi(Zn_{1/2}Ti_{1/2})O_3$-80mol% $BaTiO_3$ (BZT-BT) were synthesized through a solid-state mixed oxide approach. Bi_2O_3 (≥99.9%, Sigma-Aldrich), ZnO (≥99.0%, Sigma-Aldrich), TiO_2 (≥99.0%, Strem Chemicals), and $BaCO_3$ (≥99.0%, Sigma-Aldrich) were batched stoichiometrically without assaying powders to measure absorbed water content. Batches were ball milled in ethanol with stabilized ZrO_2 media for 24 hours, followed by drying in a rotary evaporator to minimize phase separation. The mixed oxides were calcined in filled and covered alumina crucibles. X-ray diffraction (FIG. 3-1) indicated that calcination at 850°C for 4 hours was insufficient for creating 20BZT-80BT with a phase-pure cubic perovskite structure; a second phase peak, attributed to Aurivillius-type $Bi_4Ti_3O_{12}$ or $BaBi_4Ti_4O_{15}$, appeared at $2\theta = 30°$. Increasing the calcination temperature to 950°C for 12 hours yielded phase-pure powder.

The visual appearance of the powders in the crucible after calcination was non-uniform, despite XRD results indicating the powders were phase pure; notable color variations were present in the calcined powder compact from top to bottom and exterior to interior, as well as an aggregated, “crunchy” physical state present at the top of the powder bed. Some non-uniformity of the bismuth partial pressure may have occurred despite having a filled and covered crucible,

resulting in the localized formation of point defects and/or second phases in concentrations below the detection limit of XRD.

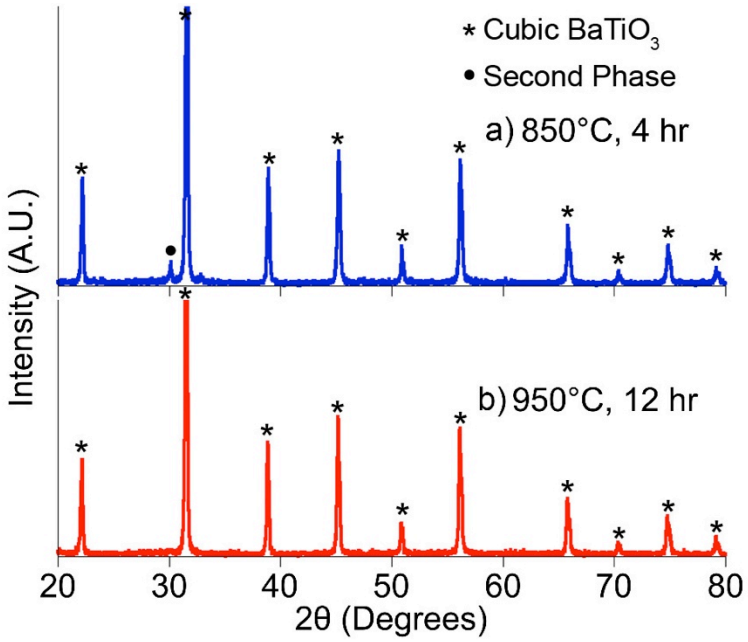

FIG. 3-1. XRD of multiphase 20BZT-80BT calcined at 850°C for 4 hours and single-phase 20BZT-80BT calcined at 950°C for 12 hours.

The calcined powders were then ball milled in ethanol with stabilized ZrO_2 media for 24 hours to break apart sintered particle aggregates created during calcination. The resultant powders had an average particle size of 800nm, determined by dynamic light scattering (Zetasizer, Malvern Instruments). A representative SEM image (Supra, Carl Zeiss International) of the calcined powder is shown in FIG. 3-2; both soft agglomerates and hard aggregates can be seen, with the latter distinguished by the presence of necking and/or grain boundaries between particles. Primary particles were generally equiaxed.

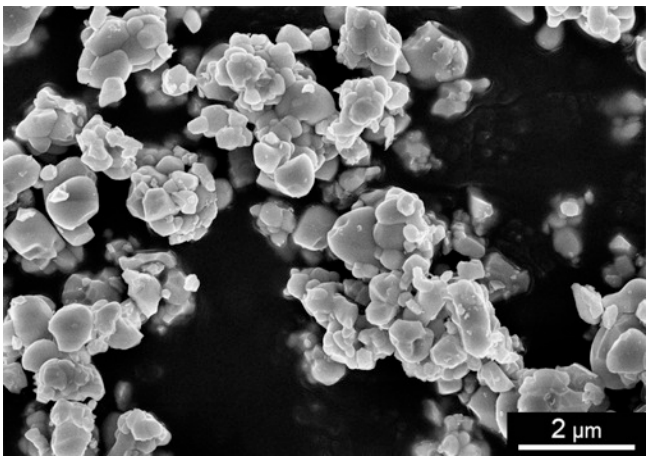

FIG. 3-2. Representative image of 20BZT-80BT particles after calcination at 950°C for 12 hours.

Two glasses, a bismuth-zinc-borate ($30Bi_2O_3$-$30ZnO$-$40B_2O_3$, in mol%) and bismuth borosilicate glass ($50Bi_2O_3$-$25B_2O_3$-$25SiO_2$, again in mol%) were made by stoichiometric mixing of Bi_2O_3, ZnO, B_2O_3 (≥99.0%, Alfa-Aesar), and SiO_2 (≥99.0%, Sigma-Aldrich); these powders were not assayed prior to use to determine any water absorbed from the ambient atmosphere. The batches were melted in covered crucibles at 950°C for 2-3 hours with occasional stirring. Melting was performed in alumina crucibles, as attempts at using platinum crucibles resulted in the reduction of the melts and the subsequent formation of non-amorphous phases. The glasses were poured and quenched between copper plates. Visual observation of the glasses during pouring indicated that the borosilicate viscosity was higher than the borate viscosity. On cooling, both glasses were transparent and yellow in color. To reduce the average glass particle size to <800nm for homogeneous glass distribution within the 20BZT-80BT, the quenched glasses were crushed with a mortar and pestle; crushed powders were ball milled for 24 hours and attrition milled for 2 hours with stabilized ZrO_2 media in ethanol. Particle size measurements conducted by dynamic light scattering (Zetasizer, Malvern Instruments) indicated that this milling process yielded glass particles averaging several microns in diameter, which was larger than desirable.

Gravitational sedimentation was employed to extract the finer glass particles. Stokes' Law calculations were performed to determine the minimum times required to settle out particles with diameters larger than 800nm. Between 5-10g of the glass powders were dispersed in ethanol with 1wt% polyvinylpyrrolidone. These particles were then added to the top of a sedimentation cone filled with ethanol, and allowed to settle. After the calculated time had passed (several hours for >10cm sedimentation height), the supernatant was extracted with a syringe. Dynamic light scattering analysis performed on particles dispersed in the supernatant indicated an average particle diameter of <600nm. The dispersions were then dried to extract the glass particles.

3.2. GLASS THERMAL CHARACTERIZATION

The $30Bi_2O_3$-30ZnO-$40B_2O_3$ and $50Bi_2O_3$-$25B_2O_3$-$25SiO_2$ glasses were analyzed with differential thermal analysis (DTA) to obtain information on the glass transition temperature (T_g), and the formation and melting temperatures (T_x and T_{melt}, respectively) of any crystalline phases formed. Measurement of these key temperatures was used for initial screening of glass viability for liquid phase sintering. The existence of any crystallization events might suggest the formation of a transient liquid phase during sintering with BZT-BT.

Powder samples of each glass were placed in alumina crucibles and heated in air to 800°C at a rate of 5°C/min with a Netzsch STA409 DTA. DTA was not performed at temperatures greater than 800°C, as higher temperatures led to the glasses wetting the crucibles so favorably that they could exit the crucibles and damage the DTA sample holder.

DTA scans for both glasses are shown in FIG. 3-3. The borate glass shows an observable endothermic event on heating to 418°C associated with T_g. This value agrees well with the 414°C glass transition reported by Kim, *et al.* for the $30Bi_2O_3$-30ZnO-$40B_2O_3$ composition.[25] Also, a sharp exothermic crystallization peak occurs at 620°C, followed by an endothermic

melting peak at 680°C. The borosilicate shows a slope change (T_g) at 416°C, and no clear events associated with crystalline phase formation or melting up to 800°C. This contrasts with the results from Huebner and Zhang, which indicated a T_g of 370°C for the same glass composition.[24]

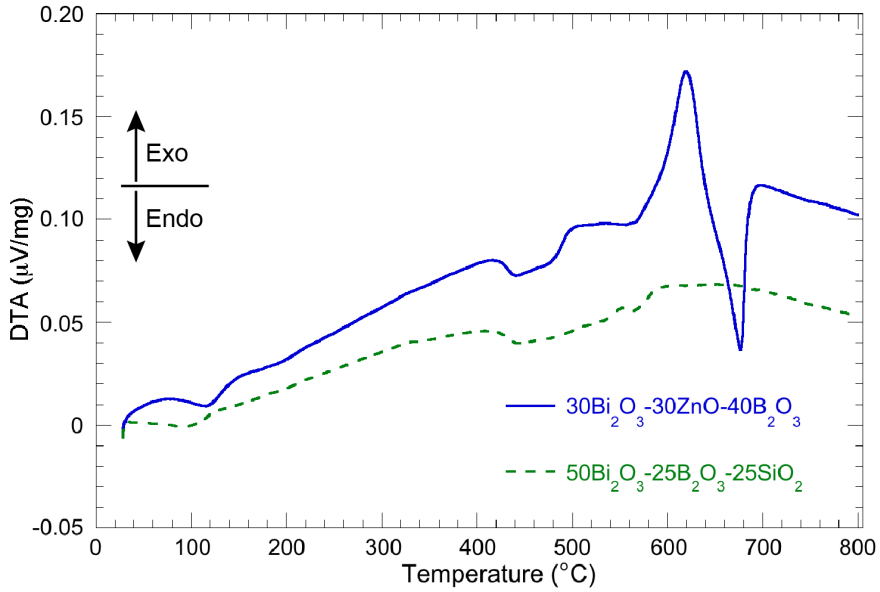

FIG. 3-3. DTA scans for the $30Bi_2O_3$-$30ZnO$-$40B_2O_3$ and $50Bi_2O_3$-$25B_2O_3$-$25SiO_2$ glasses on heating to 800°C.

A cursory investigation of the phases formed during the crystallization of the $30Bi_2O_3$-$30ZnO$-$40Bi_2O_3$ glass was limited to the use of the ternary phase diagram for the Bi_2O_3-ZnO-B_2O_3 system (shown in FIG. 3-4). The borate glass composition lies within the $Zn_3B_2O_6$-$ZnBi_4B_2O_{10}$-$Bi_3Bi_5O_{12}$ phase field, suggesting that a mixture of the three phase field components would form on recrystallization. More thorough investigations into the crystallization behavior of the glass itself were not performed in order to allow deeper study into the sintering behavior and dielectric properties of BZT-BT dielectrics sintered with additions of these glasses. Also, visual observations indicated that the crystallization behavior of the glasses was affected by particle

size, as particulate samples tended to crystallize while solid bulk samples did not. Further studies into the effect of particle size on crystallization behavior, however, were not undertaken.

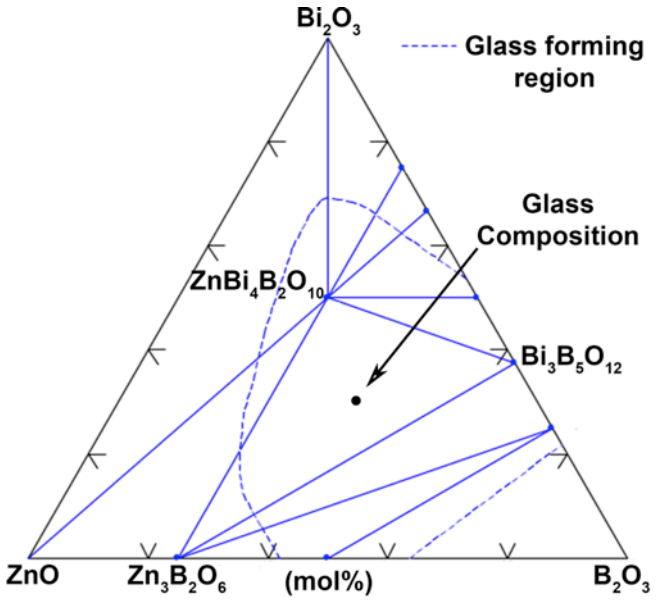

FIG. 3-4. Bi_2O_3-ZnO-B_2O_3 phase diagram showing phases likely formed during crystallization of the $30Bi_2O_3$-30ZnO-$40Bi_2O_3$ glass. (Diagram from ACerS-NIST.[26])

3.3. GLASS WETTING BEHAVIOR ON 20BZT-80BT

For either glass to effectively assist in reducing the sintering temperature, the liquid phase(s) formed on heating must exhibit favorable wetting of the bulk 20BZT-80BT particles. The wetting behavior of each glass was characterized through *in situ* optical imaging and *ex situ* electron microscopy performed on glass fragments heated and cooled while in contact with a dense sample of BZT-BT. *In situ* observations of the glass contact angle as a function of temperature macroscopically indicated the temperatures necessary for favorable wetting and, thus, effective liquid phase sintering. *Ex situ* analysis allowed measurement of the final contact angle (post-cooling) and observation of the interactions that occurred at the glass/BZT-BT

interface. Observation of these interactions indicated the formation of crystalline phases at the interface; these phases would also likely form and persist in a BZT-BT dielectric component liquid phase sintered with the glasses being studied.

3.3.1. *In Situ* Wetting Behavior. The wetting behavior of the $30Bi_2O_3$-$30ZnO$-$40B_2O_3$ and $50Bi_2O_3$-$25B_2O_3$-$25SiO_2$ glasses was characterized *in situ* with optical photography. A small piece (approximately 2mm on a side) of each glass was placed on top of a 12.7mm diameter 20BZT-80BT pellet previously sintered at 1180°C for 12 hours (geometric pellet densities were >94% of theoretical) and rough ground to a 320 grit finish. The pellet/glass samples were placed on an alumina D-tube in a tube furnace and heated in air at 3°C/min to 700°C for the borate glass and 800°C for the borosilicate. A Nikon D5000 digital camera with a 300mm zoom lens was used to collect images during heating, with the corresponding sample temperatures measured using a Type K thermocouple immediately adjacent to the sample.

A series of photographs showing the change in shape of the $30Bi_2O_3$-$30ZnO$-$40B_2O_3$ glass sample is shown in FIG. 3-5. Minimal changes occurred on heating to 511°C. By 552°C, the glass had softened, allowing surface tension to reshape the sample into a droplet. Between 582°C and 670°C, the sample shape became asymmetric, possibly indicating the heterogeneous nucleation of a crystalline phase at the sample/BZT-BT interface that interfered with spreading of the glass. Formation of a crystalline phase between 582-670°C was consistent with the crystallization exotherm observed at 620°C in the DTA scans shown previously in Section 3.2. Between 670°C and 685°C, the sample melted and completely covered the pellet surface and sides, confirming favorable wetting of the 20BZT-80BT; this, again, was consistent with the 680°C melting temperature indicated by the borate DTA scan in Section 3.2. The pellet reached a maximum temperature of 692°C before cooling to room temperature.

Images of the borosilicate on BZT-BT during heating (FIG. 3-6) indicated gradual softening and favorable wetting on heating to 800°C.

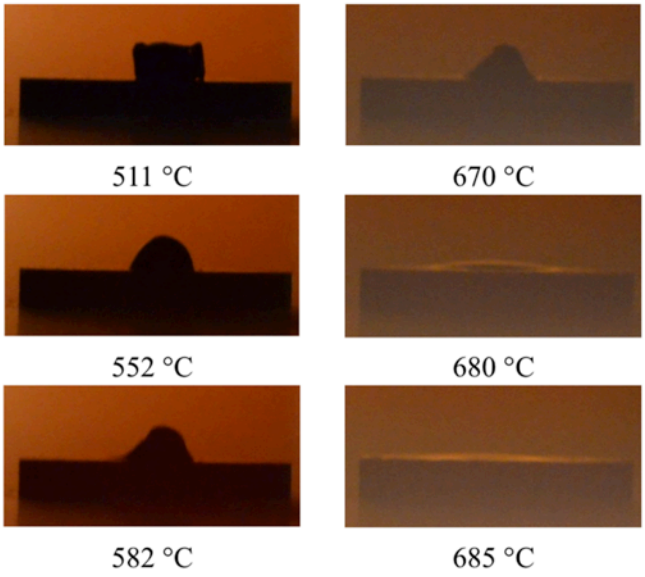

FIG. 3-5. *In situ* photographs showing wetting behavior of the $30Bi_2O_3$-30ZnO-$40B_2O_3$ glass during heating on a BZT-BT pellet to 700°C.

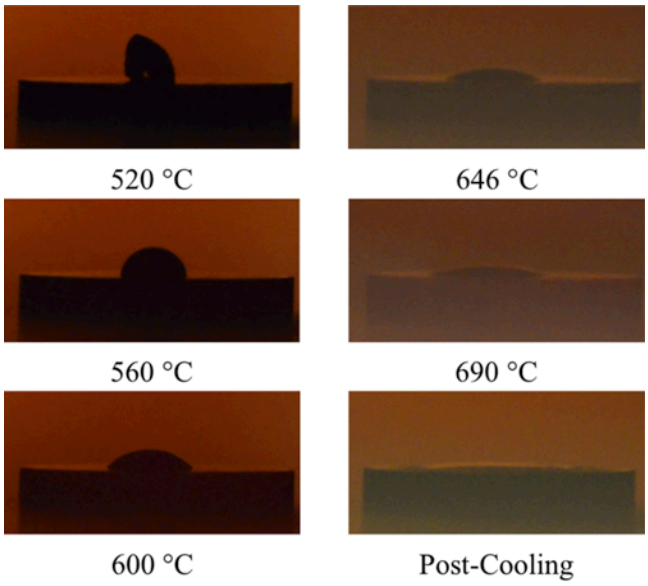

FIG. 3-6. *In situ* photographs showing wetting behavior for the $50Bi_2O_3$-$25B_2O_3$-$25SiO_2$ glass on a BZT-BT surface during heating to 800°C.

The favorable wetting behavior exhibited by both glasses below 800°C suggested that the glasses would be able to spread throughout the grain boundaries and porosity in a low-density BZT-BT dielectric at temperatures well below the 1180°C sintering temperature used for the pure dielectric.

3.3.2. *Ex Situ* Characterization. The glass/BZT-BT pellet samples used for *in situ* wetting angle observations were cut in cross-section and polished to allow imaging of the glass-pellet interface via scanning electron microscopy with a Zeiss Supra SEM.

The $30Bi_2O_3$-$30ZnO$-$40B_2O_3$ glass exhibited a contact angle of ≈6° after cooling from 700°C, as shown in FIG. 3-7. Backscatter electron imaging revealed that, in addition to thorough wetting of the BZT-BT pellet surface, the borate glass crystallized into a bright, high-Z (high atomic number) phase at the glass/BZT-BT interface (shown in FIG. 3-8). This phase formed long columnar crystallites. Furthermore, the liquid phase penetrated several grains below the pellet surface, as evidenced by the presence of "floating" grains near the surface.

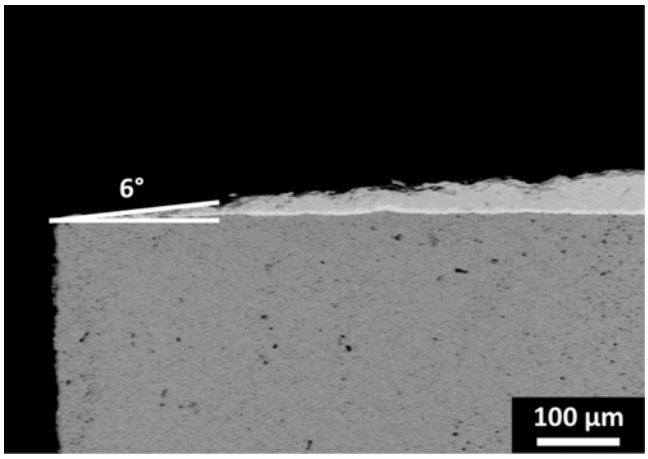

FIG. 3-7. Contact angle measurement of 6° made on the $30Bi_2O_3$-$30ZnO$-$40B_2O_3$ glass after heating to 700°C on a BZT-BT pellet.

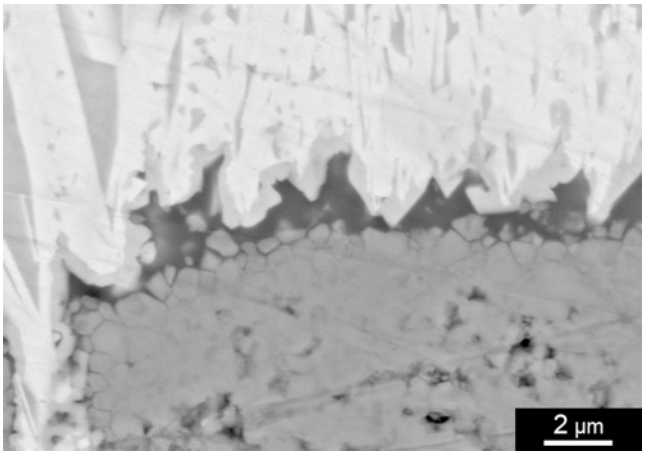

FIG. 3-8. Backscatter electron image showing crystallization layer formed at the interface between the $30Bi_2O_3$-30ZnO-$40B_2O_3$ glass and BZT-BT pellet after heating to 700°C.

Energy dispersive spectroscopy element mapping (FIG. 3-9) indicated that the crystalline layer was approximately 10µm thick and contained bismuth, titanium, and possibly barium, while being deficient in zinc. The glass itself was rich in bismuth and zinc only, and the dark amorphous phase between the crystalline phase and the 20BZT-80BT contained zinc, barium, and titanium.

The crystalline phase is suspected to be an Aurivillius-type bismuth titanate ($Bi_4Ti_3O_{12}$, or similar) or barium bismuth titanate phase, based on the high-aspect ratio crystallite geometry, elemental composition, and evidence of these phases in BZT-BT pellets sintered with inhomogeneously distributed borate glass.[27,28] However, a significant overlap exists between the EDS peaks for Ba and Ti; this overlap obscures the actual Ba or Ti content in the crystallites and makes accurate determination of the crystallite composition difficult.

The Bi_2O_3-TiO_2 phase diagram, shown in FIG. 3-10, can be combined with the information gained from SEM/EDS analysis to indicate a potential reaction sequence leading to the formation of persistent $Bi_4Ti_3O_{12}$ (BiT) crystals at the borate/BZT-BT interface. During

heating, Ti is suspected to have diffused out of the BZT-BT into the borate glass, leading to the initial formation of BiT crystallites at the glass/pellet interface.

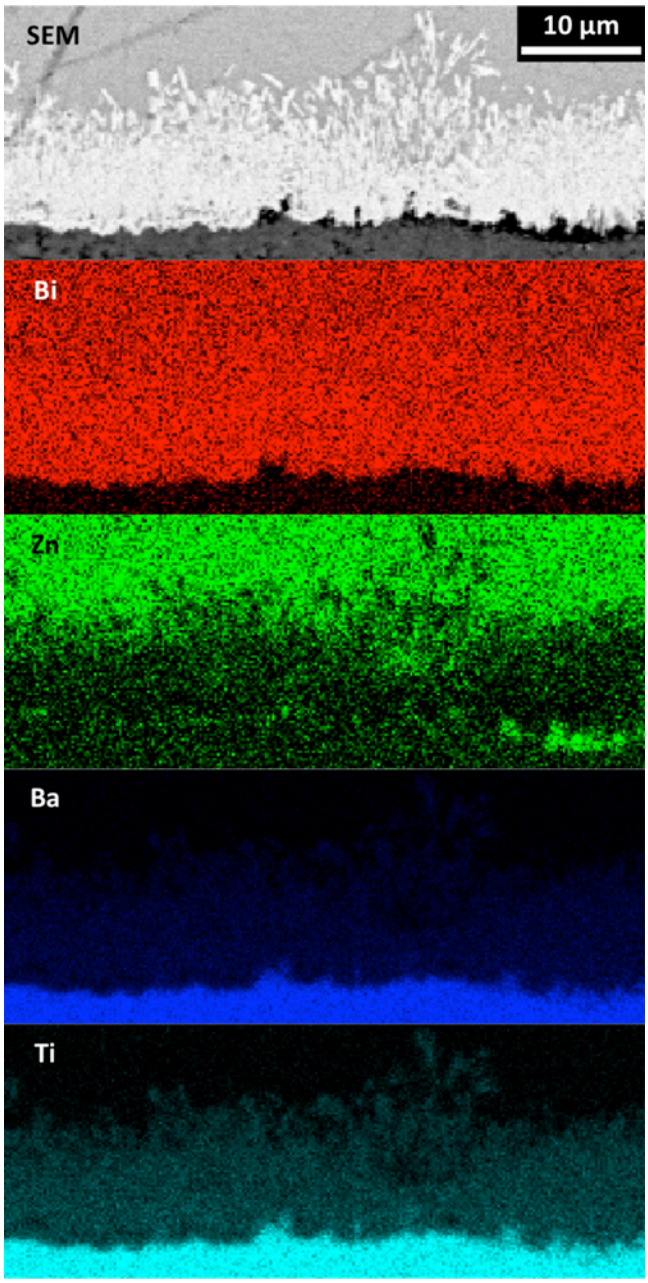

FIG. 3-9. EDS element maps showing chemical composition of the high-Z crystallized phase at the interface between the $30Bi_2O_3$-30ZnO-$40B_2O_3$ glass and BZT-BT pellet after heating to 700°C.

Formation of the BiT in turn removed Bi from the glass, leaving behind a Bi-deficient $ZnO\text{-}B_2O_3$ glass (dark amorphous phase near interface). As the reaction progressed, the increased number and size of BiT crystals formed a barrier layer that hampered further Ti diffusion into the glass, stopping further nucleation of BiT crystals approximately 10μm from the final glass/BZT-BT interface.

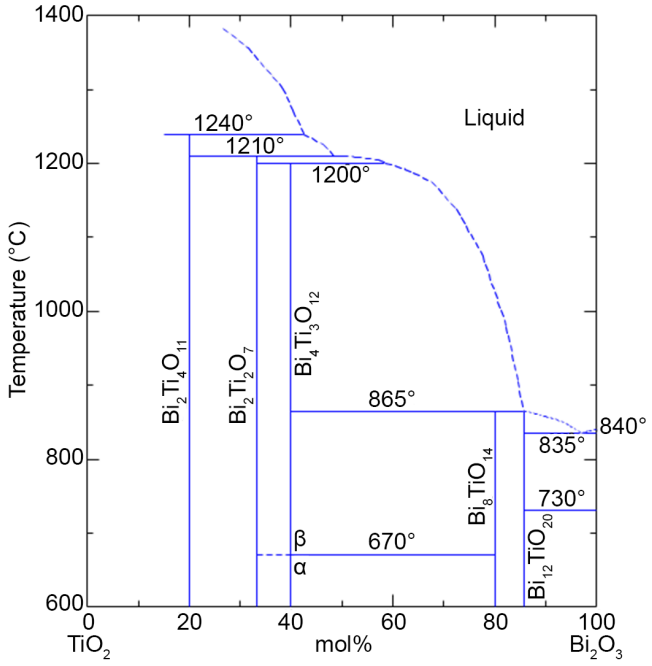

FIG. 3-10. $Bi_2O_3\text{-}TiO_2$ phase diagram. (Diagram from ACerS-NIST.[29])

Whether the glass actually dissolved portions of the BZT-BT surface is unknown, but the crystallites were observed to have grown into pores and voids on the BZT-BT surface. The phase diagram for $Bi_2O_3\text{-}TiO_2$ indicates that Bi-rich compositions near $Bi_4Ti_3O_{12}$ do not begin to melt until heating above 865°C; as such, any BiT or similar compositions would remain after heating the wetting angle sample to 700°C. BiT crystals are ferroelectric, and their presence in a liquid

phase sintered dielectric after cooling would be desirable for formation of a transient liquid phase.[30]

A contact angle of ≈10° was measured between the $50Bi_2O_3$-$25B_2O_3$-$25SiO_2$ glass and BZT-BT surface (FIG. 3-11). The borosilicate melt also appeared to have penetrated the grain boundaries in the BZT-BT near the surface, as shown by backscatter electron imaging in FIG. 3-12. A crystallization layer approximately 5μm thick formed at the glass-pellet interface; the crystalline phase was a low-Z (dark) phase, as opposed to the high-Z phase formed by the $30Bi_2O_3$-$30ZnO$-$40B_2O_3$ glass.

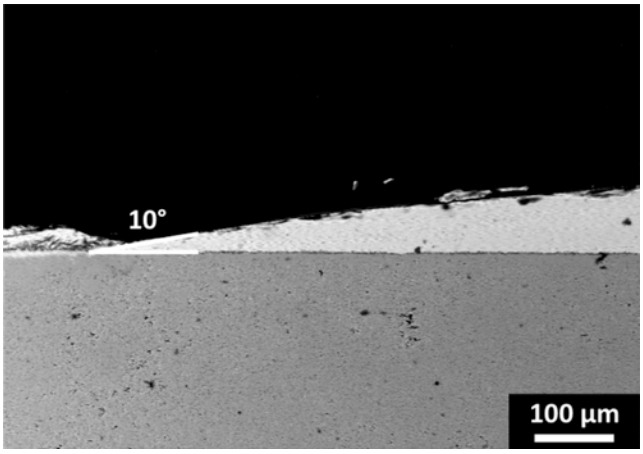

FIG. 3-11. Contact angle measurement of 10° made on the $50Bi_2O_3$-$25B_2O_3$-$25SiO_2$ glass after heating to 800°C on a BZT-BT pellet.

An EDS point spectrum collected on the low-Z phase, shown in FIG. 3-13, indicated the presence of Ba, Al, and Si, suggesting the formation of a barium silicate or barium aluminosilicate phase; Ti may also be present within the crystallites due to the EDS peak overlap between Ba and Ti discussed previously. The presence of Al is attributed to glass contamination

caused by dissolution of the alumina crucibles used for melting, as no other sources of alumina contamination existed during material processing.

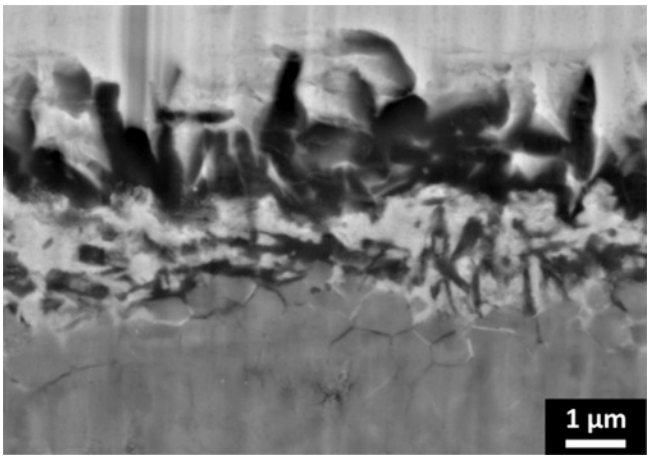

FIG. 3-12. Backscatter electron image showing low-Z crystallized phase at the interface between the borosilicate glass and BZT-BT pellet after heating to 800°C.

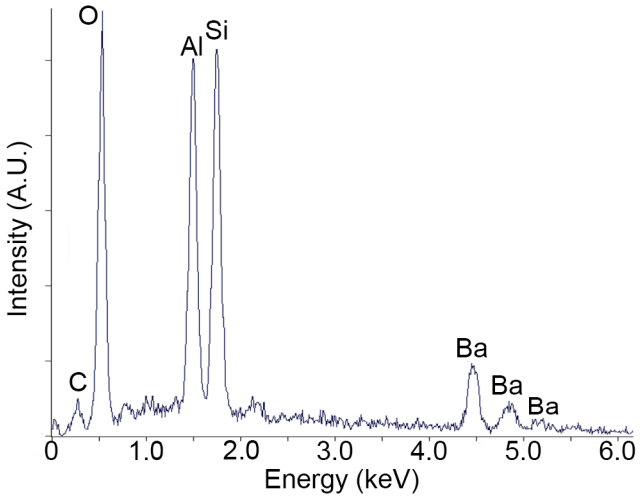

FIG. 3-13. EDS point spectrum from the dark crystalline phase at the interface between the borosilicate glass and BZT-BT pellet.

A process similar to the suggested formation of BiT can be proposed for creating a barium silicate crystalline phase at the borosilicate/BZT-BT interface. In this case, Ba must be transported from the BZT-BT surface and into the Bi-borosilicate glass. Crystallites of a barium silicate (possibly $BaSiO_3$ or, more generically, $(Ba,Ti)SiO_x$) phase formed at the interface, slowing diffusion of the Ba into the glass and preventing further crystallite formation. The higher viscosity of the borosilicate glass relative to the borate glass also likely contributed to slower Ba diffusion and thus formation of a thinner crystallization layer (≈5μm thick). The BaO-SiO_2 phase diagram, shown in FIG. 3-14, reveals that none of the possible barium silicate phases melt below 1374°C; as such, the barium silicate crystallites that nucleate would persist at the interface during the wetting angle studies up to 800°C.

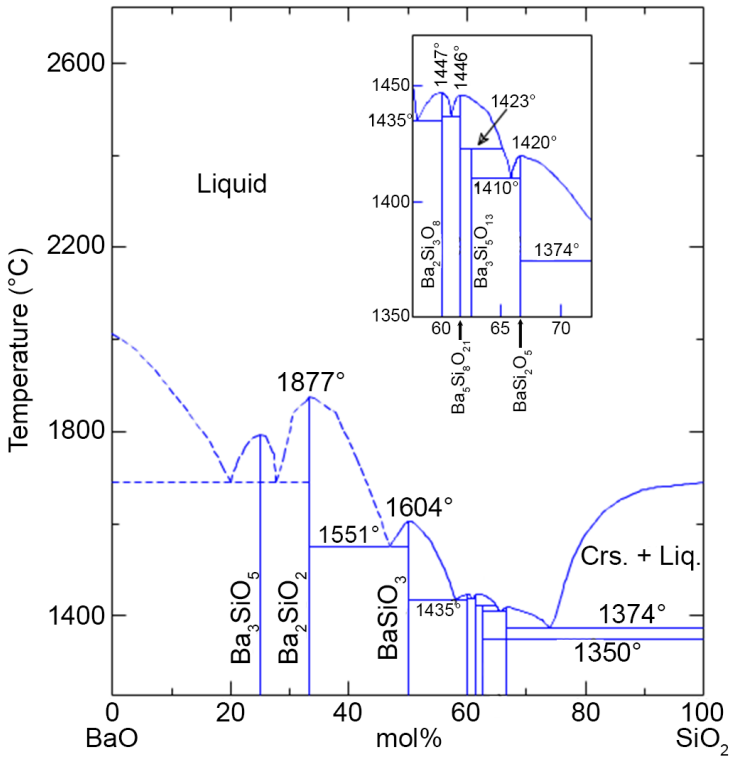

FIG. 3-14. BaO-SiO_2 phase diagram. (Diagram from ACerS-NIST.[31])

Since both glasses exhibited wetting angles of ≤10°, attacked the grain boundaries of the BZT-BT near the interface, and crystallized at the glass/BZT-BT interface, these glasses were considered to be viable candidates for formation of a transient liquid phase useful for sintering at reduced temperatures.

3.4. GLASS/BZT-BT POWDER MIXTURE THERMAL ANALYSIS

Following the discovery of crystalline layers at the glass/BZT-BT interfaces, differential thermal analysis was employed in an effort to determine the temperatures required for crystallization of the observed phases. Measurement of exothermic transitions on heating or cooling would indicate the temperatures at which the crystalline BiT or $BaSiO_3$ phases formed on the BZT-BT grains, while endothermic transitions would indicate the melting of these phases.

Each glass powder was mixed with 20BZT-80BT powder to form compositions comprised of 5v% glass. Poly(propylene carbonate) binder (QPAC40, Empower Materials) was added in concentrations of 2-3 wt% by ball milling with stabilized ZrO_2 media in acetone. The powders were lightly packed into alumina DTA crucibles and subjected to differential thermal analysis in a Netzsch STA449 F1 Jupiter unit. Samples were heated to and cooled from 1000°C in air at a heating/cooling rate of 5°C/min.

The DTA curves in FIG. 3-15 show several thermal events on heating of the 5v% glass + BZT-BT mixtures. The dominant exotherms occurring in both samples from 200°C-400°C are associated with the decomposition and volatilization of the poly(propylene carbonate) binder. With further heating, a small exothermic rise appears for both glass-containing samples at 780°C. The 5v% $50Bi_2O_3$-$25B_2O_3$-$25SiO_2$ + BZT-BT glass sample curve shows several other small exotherms at 500°C and 570°C, which correspond to two small exotherms in the DTA curve for the borosilicate glass. Notably absent are any strong exotherms or endotherms associated with

crystallization or melting of either glass, though such events may be obscured due to the small amount of glass present in the samples. Mixtures of 50wt% glass-50wt% BZT-BT were initially used in an attempt to amplify the signals associated with any obscured events, but severe wetting of the crucibles by the glass-BZT-BT mixtures led to equipment damage and discontinuation of studies of mixtures with high glass concentrations.

On cooling (FIG. 3-16), the DTA curve for the sample containing 5v% $30Bi_2O_3$-30ZnO-$40B_2O_3$ shows a small exotherm at 880°C. Neither DTA curve indicates any discernable thermal event associated with recrystallization of the either glass on cooling, but, again, the volume fraction of each glass (5v%) is sufficiently small that any such events are likely obscured.

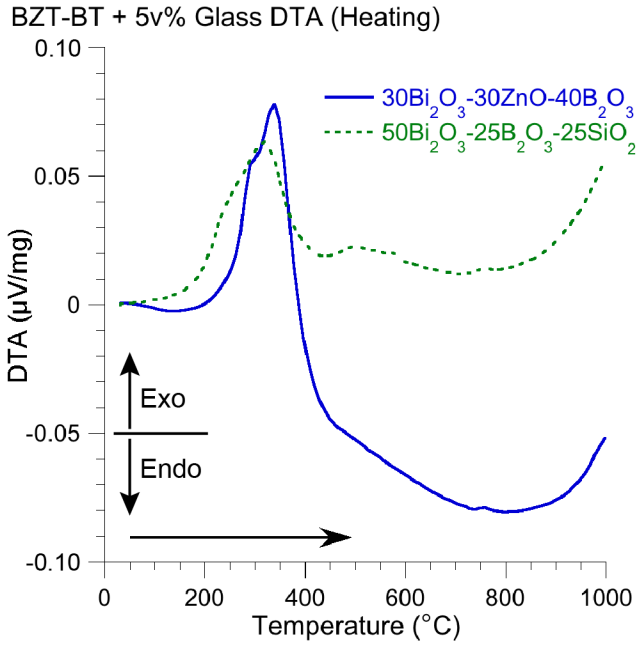

FIG. 3-15. Differential thermal analysis curves for heating of 20BZT-80BT samples containing 5v% $30Bi_2O_3$-30ZnO-$40B_2O_3$ or $50Bi_2O_3$-$25B_2O_3$-$25SiO_2$ glass.

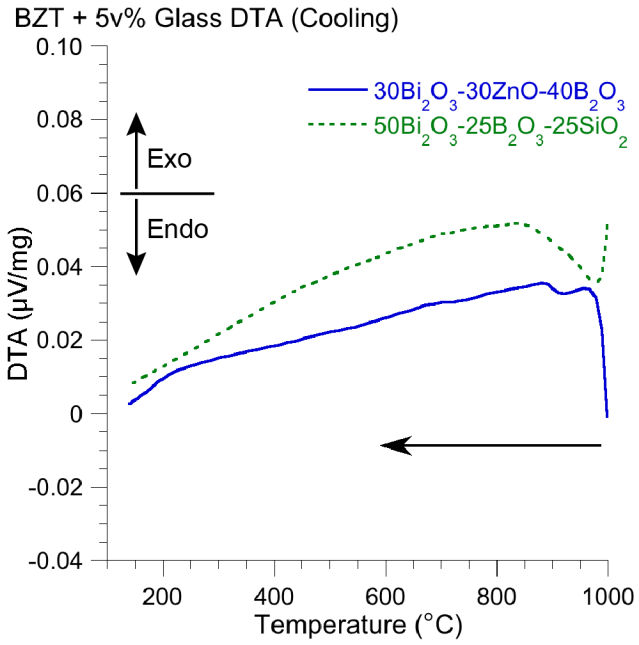

FIG. 3-16. Differential thermal analysis curves for 20BZT-80BT samples containing 5v% $30Bi_2O_3$-30ZnO-$40B_2O_3$ or $50Bi_2O_3$-$25B_2O_3$-$25SiO_2$ on cooling from 1000°C.

4. DENSIFICATION AND MICROSTRUCTURAL EVOLUTION

After gaining a preliminary understanding of the interactions occurring between each glass and the BZT-BT dielectric, sintering studies were conducted on BZT-BT with small additions of each glass (≤ 5vol%) to study the effects of the glass additions on densification. Initial studies were conducted using a fixed sintering time (four hours) for simplicity at several temperatures to determine the lowest temperatures necessary for the glass-containing BZT-BT to reach useful density levels (≥95%) for high field dielectric applications.

4.1. DENSIFICATION STUDIES

Densification studies were conducted by fabricating and sintering 20BZT-80BT pellets containing 1, 2, and 5 vol% of either the $30Bi_2O_3$-30ZnO-$40B_2O_3$ or $50Bi_2O_3$-$25B_2O_3$-$25SiO_2$ glasses. Each glass was added to the 20BZT-80BT in appropriate amounts for each mixture; these powders were mixed in plastic bottles with 1-3 wt% poly(propylene carbonate) binder (QPAC40, Empower Materials) in acetone using stabilized ZrO_2 media. The mixtures were placed in a heated drying oven at 65°C and allowed to dry. The dry powders were passed through a No. 20 sieve, and pressed into 12.7mm diameter pellets by uniaxial die pressing. Cold isostatic pressing of the pellets to a pressure of 152 MPa yielded samples with geometric green densities of 59-63% relative to 20BZT-80BT theoretical. Two or three samples of each composition were sintered in sacrificial 20BZT-80BT powder beds at 700°C, 800°C, 950°C, and 1000°C for four hours at a heating rate of 5°C/min. Temperatures were selected based on densification rate changes measured by dilatometry. Bulk densities of the samples were measured with the Archimedes technique via vacuum infiltration with kerosene (results shown in FIG. 4-1).

Bulk densities for pellets sintered at 700°C are shown as a function of glass composition and concentration in FIG. 4-1a. At 700°C, samples containing the $30Bi_2O_3$-30ZnO-$40B_2O_3$ glass

obtained densities between 73-75%, representing a 2-5% improvement over pure 20BZT-80BT samples sintered at the same conditions. The improvement is attributed to Stage I liquid phase sintering, as the molten borate glass began to fill the interstices between BZT-BT particles while also allowing BZT-BT particle rearrangement. The $50Bi_2O_3$-$25B_2O_3$-$25SiO_2$-containing samples reached a lower density (≈67%) than the borate-containing samples, likely due to limited particle rearrangement and filling of porosity by the higher viscosity borosilicate glass. The difference in relative densities between the glass-containing samples and non-glass containing samples was not due to differences between the pure glass and 20BZT-80BT densities. The densities of the pure glasses (6.5-6.7 g/cm^3, as measured by the Archimedes technique) were approximately the same as pure 20BZT-80BT (6.419 g/cm^3, calculated from XRD lattice parameters).

FIG. 4-1b shows the relative densities of samples sintered at 800°C for four hours. After sintering at 800°C, the 20BZT-80BT samples achieved higher relative densities than samples containing all glass compositions and concentrations. As with the 700°C densities, the borosilicate-containing sample densities are slightly lower than for the borate-containing samples. Also, samples containing 1v% of each glass reached the highest relative densities of all of the glass concentrations. All liquid phase sintered sample densities were slightly less than the densities of the pure 20BZT-80BT samples sintered at 800°C. This could be due to the formation of the crystalline phases expected to form at the glass/BZT-BT interfaces (described in Section 3.3.2); if formed on heating, these crystalline phases may actually hamper densification by interfering with matter transfer between the BZT-BT grains.

Relative densities achieved after sintering at 950°C are shown in FIG. 4-1c. Samples containing the $30Bi_2O_3$-$30ZnO$-$40B_2O_3$ glass reached higher densities than samples containing the borosilicate, though samples containing either glass at the 5v% concentration level obtained nearly equivalent densities. The 2v% concentrations reached the lowest densities for both glass systems.

FIG. 4-1d shows the relative densities of samples sintered at 1000°C for four hours. Samples containing all borate concentrations reached relative densities around 95%, while only the 5v% borosilicate samples reached the 95% relative density level; these densities represent a 5% improvement over pure 20BZT-80BT. As with the samples sintered at 950°C, the borosilicate sample densities lag behind those of the borate samples at the 1v% and 2v% concentrations. Samples containing 2v% glass again exhibited the lowest densities of all concentrations for both glasses.

The relatively large increase in density (≈15%) of the borate-containing samples from 800°C-1000°C was attributed to the melting of the bismuth titanate crystalline phase(s). The phase diagram for the Bi_2O_3-TiO_2 system (shown previously in FIG. 3-10) indicated that compositions between the $Bi_4Ti_3O_{12}$ (BiT) and Bi_8TiO_{14} compounds begin to melt at temperatures above 865°C. If these crystalline phases indeed hamper sintering by interfering with diffusion and transport processes through the liquid phase, or at the very least reduce the amount of liquid phase available, sintering at temperatures above the crystal phase melting temperature would yield improved densification. Such improvements were realized by the density increase between sintering at 800°C and 1000°C.

Similar reasoning also provided an explanation for the generally lower densities of the borosilicate-containing samples. The formation of barium silicate crystalline phases such as $BaSiO_3$ along the surfaces of the BZT-BT particles may also hinder densification by interfering with matter transport or reducing the amount of liquid phase available to aid in sintering. None of the barium silicate phases on the BaO-SiO_2 phase diagram (shown previously in FIG. 3-14) melt below 1374°C. Sintering temperatures of 1000°C or less would thus be insufficient to melt the crystalline phases (unless a eutectic phase formed through reaction of the crystalline phase and BZT-BT), yielding reduced density improvements between 800°C-1000°C.

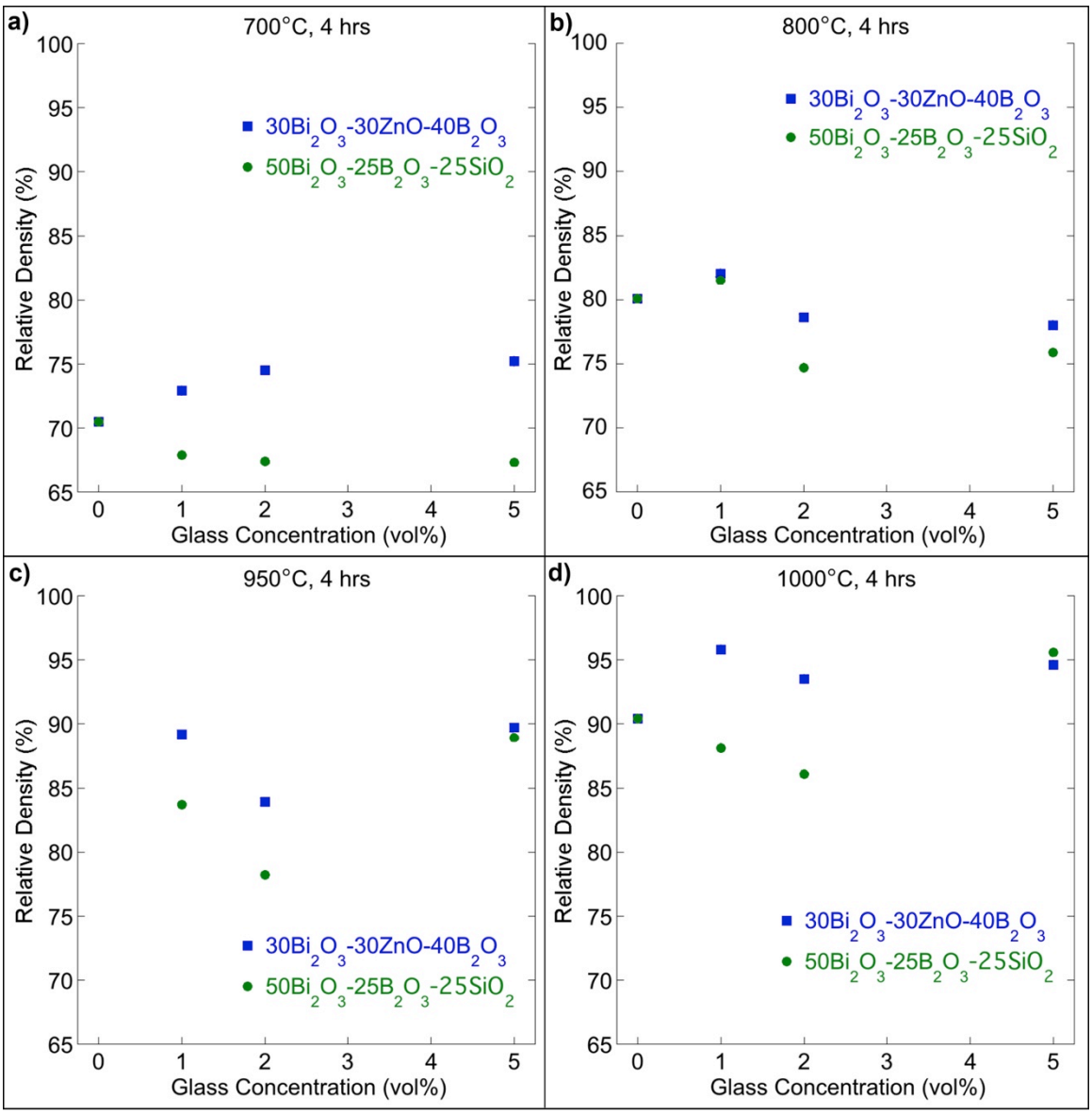

FIG. 4-1. Relative densities of 20BZT-80BT pellets containing $30Bi_2O_3$-30ZnO-$40B_2O_3$ and $50Bi_2O_3$-$25B_2O_3$-$25SiO_2$ glass sintered at 700°C, 800°C, 950°C, and 1000°C for four hours.

Since samples containing 5v% borosilicate achieved relative densities >95%, samples with higher initial glass concentrations may lie in a different phase field on the unknown BZT-BT-borosilicate phase diagram, or may have a sufficiently high glass concentration that the relative amount of crystalline phase formed is small and does not drastically affect sintering.

Viscosity reductions with heating from 800°C to 1000°C could also be responsible for improved densification.

Since the samples containing 1, 2, and 5v% $30Bi_2O_3$-30ZnO-$40B_2O_3$ and 5v% $50Bi_2O_3$-$25B_2O_3$-$25SiO_2$ reached ≈95% theoretical densities after sintering at 1000°C for four hours, these four compositions and concentrations are believed to be promising candidates on the basis of densities alone. These samples approached useful density levels for capacitor dielectrics at a temperature 180°C lower than the sintering temperature for pure 20BZT-80BT. Further study of the impact of sintering time on the densities of these liquid-phase sintered parts could yield even more useful data, allowing parts to be sintered to full density (99% of theoretical) at 1000°C.

4.2. MICROSTRUCTURAL EVOLUTION

Microstructural imaging was performed on sintered glass-containing pellets to observe liquid phase distribution and microstructural evolution as a function of sintering temperature. Samples with 5v% glass additions were chosen for scanning electron microscopy studies (S4700, Hitachi High Technologies America and Supra, Carl Zeiss Microscopy); such samples should contain the highest volume of liquid phase and allow easier observation of the liquid phase distribution.

Samples sintered at 700°C, 800°C, and 1000°C for four hours (not exposed to kerosene from the bulk density measurements) were mounted in epoxy and polished to a surface finish of 0.25μm using a combination of SiC polishing papers and water-based diamond suspensions. No solvents were used during the polishing process that could dissolve and smear the epoxy into the porous low sintering temperature samples. Polished samples were then ultrasonicated in water and acetone and baked for 12 hours at 60°C to remove any possible contaminants prior to imaging.

FIG. 4-2 shows the fractured surface of a pellet in the green state; all sintered pellets started in the green state with a relative geometric density of 59-64% of theoretical for 20BZT-80BT. Visible grains had an average grain size of approximately 750-800nm. Some larger grains and sintered aggregates still remained, despite the ball milling procedures.

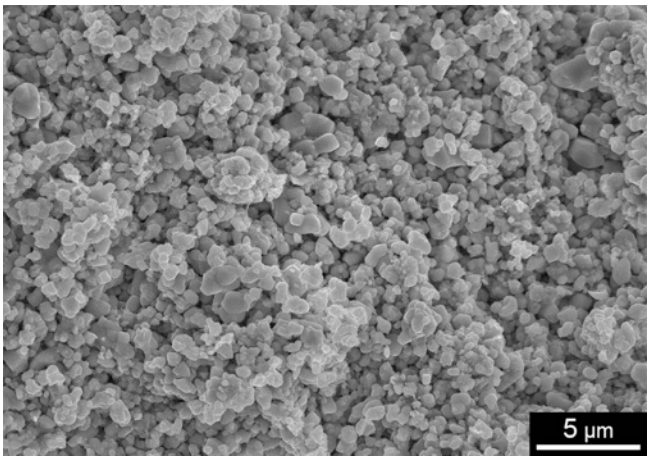

FIG. 4-2. Green state microstructure representative of all pellet compositions studied.

Microstructures of polished pellets sintered at 700°C for four hours are shown in FIG. 4-3. In keeping with the bulk density trends, the microstructure of the 5v% $30Bi_2O_3$-30ZnO-$40B_2O_3$ sample (FIG. 4-3a) appeared to be more dense than the 5v% $50Bi_2O_3$-$25B_2O_3$-$25SiO_2$ (FIG. 4-3b) and pure 20BZT-80BT (FIG. 4-3c) samples, as evidenced by the flat, polished "islands" present only in FIG. 4-3. These islands, which were secure enough to survive the polishing process without grain pullout, were likely where particles of the borate glass had melted and locally aided in sintering and particle rearrangement; since the sintering temperature was only 20°C above the glass melting temperature, the complete dispersal of the glass throughout the sample was unlikely.

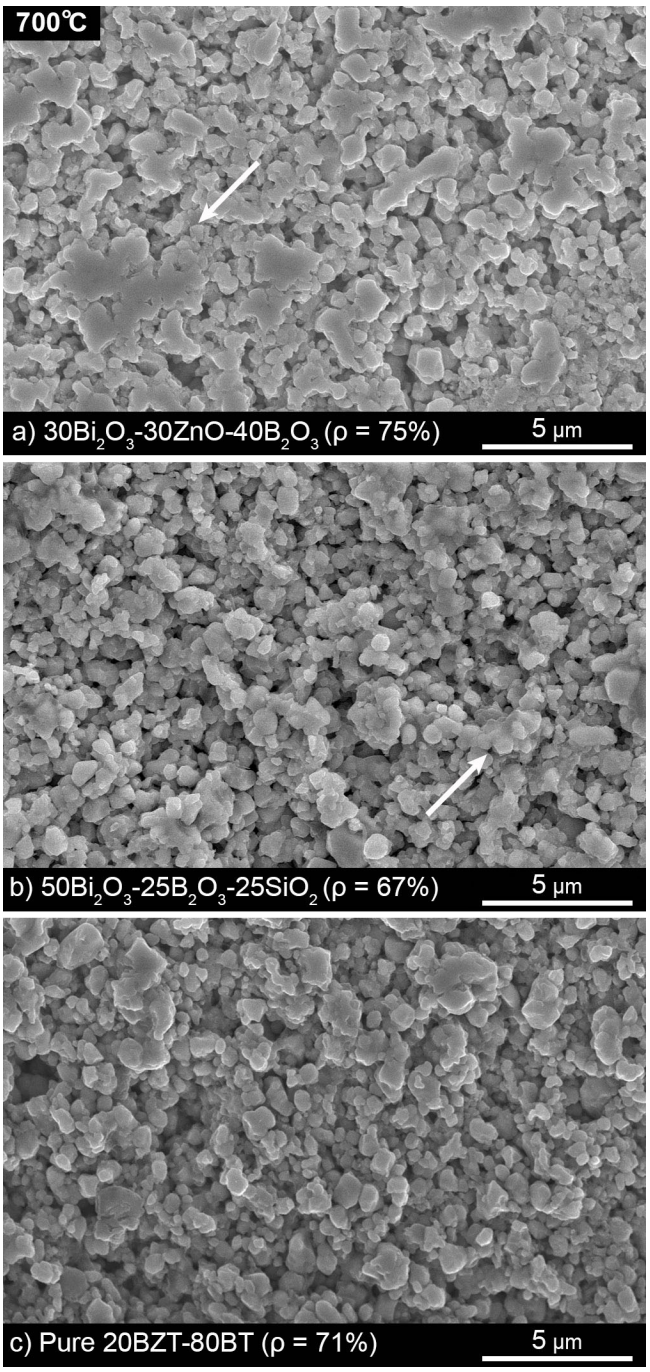

FIG. 4-3. Secondary electron images of samples containing (a) 5v% $30Bi_2O_3$-30ZnO-$40B_2O_3$, (b) 5v% $50Bi_2O_3$-$25B_2O_3$-$25SiO_2$, and (c) pure 20BZT-80BT after sintering at 700°C for four hours.

The $50Bi_2O_3$-$25B_2O_3$-$25SiO_2$ and 20BZT-80BT samples lacked these dense regions consistent with reduced particle rearrangement and sintering. Some regions in the borosilicate

sample show evidence of a glassy phase, indicating that the glass had softened but not spread throughout the sample. As expected, more open porosity was apparent in the borosilicate sample, likely caused by hampering of solid state sintering by the more viscous borosilicate glass.

The microstructures of samples sintered at 800°C for four hours are shown in FIG. 4-4. The dense islands associated with localized densification were visible in all three sample types; however, the sample containing 5v% $30Bi_2O_3$-30ZnO-$40B_2O_3$ (FIG. 4-4a) showed a significantly larger sintered (polished) area than either the $50Bi_2O_3$-$25B_2O_3$-$25SiO_2$ (FIG. 4-4b) or pure 20BZT-80BT (FIG. 4-4c) samples. By 800°C, a liquid phase film appeared throughout the borosilicate-containing sample, indicating more complete wetting of the sample as the glass viscosity decreased on heating. Curiously, a liquid phase film was also widely apparent in the pure 20BZT-80BT sample. The source of this film in the pure 20BZT-80BT sample is currently unknown; sample preparation (i.e. transfer of epoxy into sample porosity during polishing) was not responsible, given the extensive measures taken to prevent such contamination.
The source of the film is likely from a liquid phase formed from the BZT-BT itself during heating, perhaps as a compensation mechanism for excess Bi. This cannot be confirmed at this time, as no phase diagram exists for the pure BZT-BT system. However, this film likely contributed to the greater density of the pure BZT-BT relative to the glass-containing samples after sintering at 800°C.

Sintering at 1000°C for four hours (FIG. 4-5) yielded dense microstructures for samples containing 5v% $30Bi_2O_3$-30ZnO-$40B_2O_3$ (FIG. 4-5a) and 5v% $50Bi_2O_3$-$25B_2O_3$-$25SiO_2$ (FIG. 4-5b) glass, as expected from the relative density measurements. Images of the borosilicate-containing sample revealed obvious dark regions containing a number of grains; these regions are expected to be areas of high glass concentration, perhaps porosity that the glass flowed into and filled during sintering. These regions are less apparent in the borate-containing sample image.

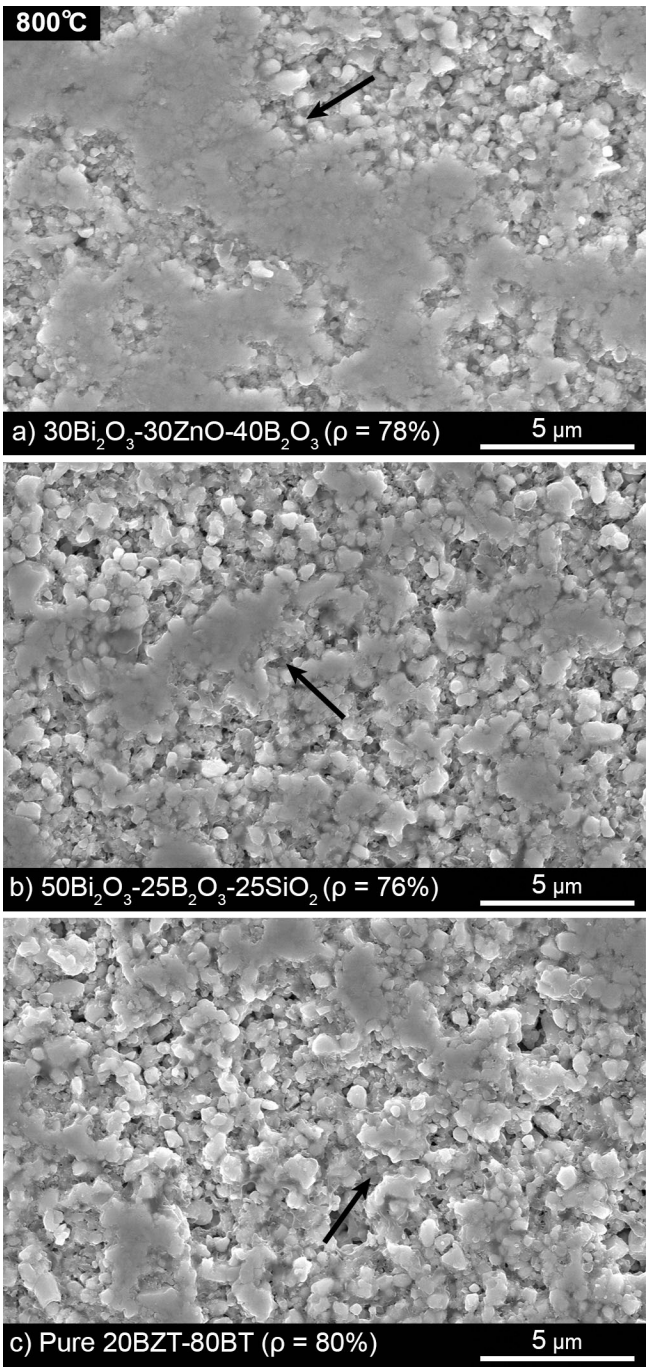

FIG. 4-4. Microstructures of samples containing (a) 5v% $30Bi_2O_3$-$30ZnO$-$40B_2O_3$, (b) 5v% $50Bi_2O_3$-$25B_2O_3$-$25SiO_2$, and (c) pure 20BZT-80BT after sintering at 800°C for four hours.

In the less dense 20BZT-80BT (FIG. 4-5c) sample, grain growth and necking are visible; the film phase observed at 800°C in the pure BZT-BT sample may be responsible.

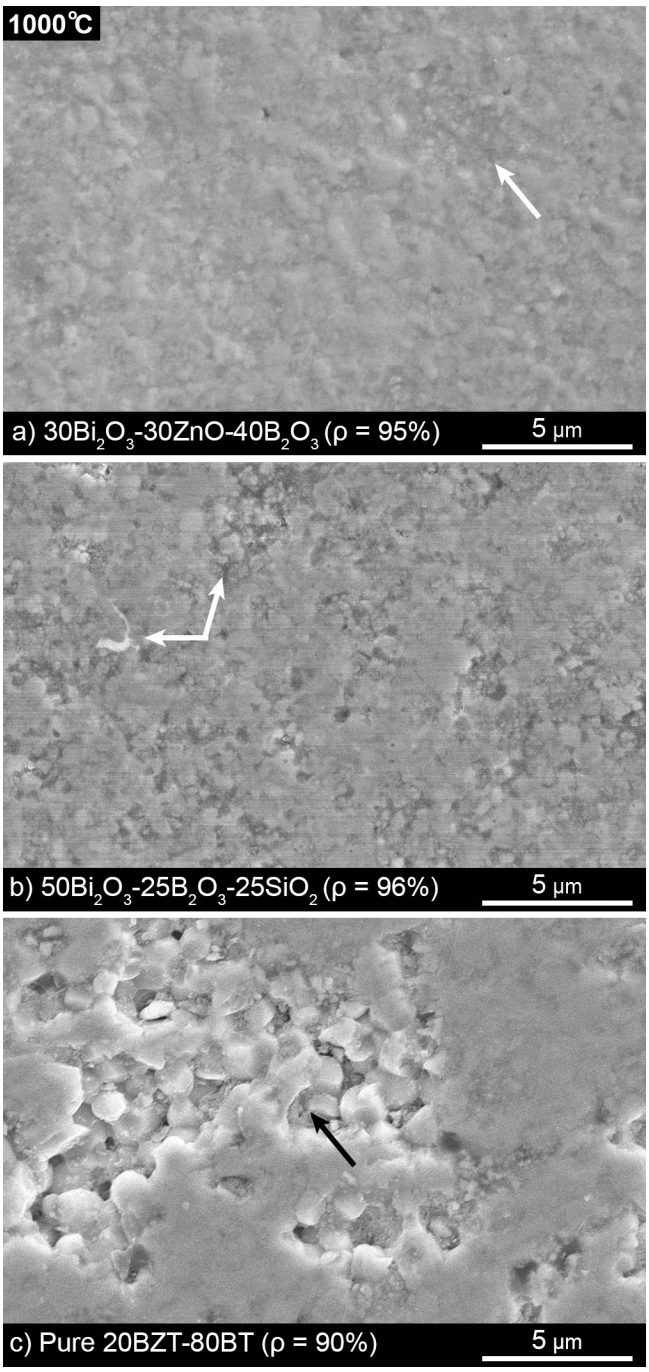

FIG. 4-5. Microstructures of samples containing (a) 5v% $30Bi_2O_3$-30ZnO-$40B_2O_3$, (b) 5v% $50Bi_2O_3$-$25B_2O_3$-$25SiO_2$, and (c) pure 20BZT-80BT after sintering at 1000°C for four hours.

As a preliminary attempt at identifying the distribution of phases present in the liquid phase sintered samples, backscatter electron imaging was performed on the dense glass-

containing samples sintered at 1000°C. These images, shown in FIG. 4-6, show mottled grain contrast characteristic of the BZT-BT bulk; it was not possible to obtain sharp images of these samples. In both liquid phase sintered samples, high-Z and low-Z second phases appear via atomic number (Z) contrast in pockets between the grains, indicating that the glasses flowed into and filled porosity within the sample.

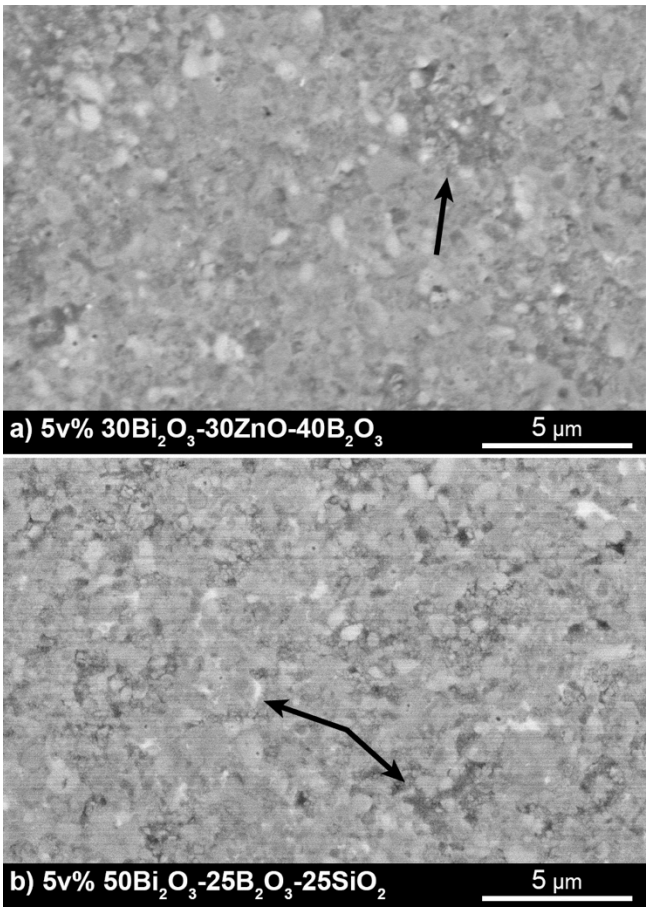

FIG. 4-6. Backscatter electron imaging showing grain and atomic number contrast in the (a) 5v% $30Bi_2O_3$-30ZnO-$40B_2O_3$ and (b) 5% $50Bi_2O_3$-$25B_2O_3$-$25SiO_2$ samples sintered at 1000°C for four hours.

4.3. SUMMARY

From these densification studies, 5v% additions of both the $30Bi_2O_3$-30ZnO-$40B_2O_3$ and $50Bi_2O_3$-$25B_2O_3$-$25SiO_2$ glasses seemed to significantly contribute to densification after sintering at 1000°C for four hours. Results indicated that this was likely due to melting of crystalline interaction phases and/or reductions in liquid viscosity. After sintering for four hours at such temperatures, 20BZT-80BT dielectrics reached 95% relative density. Further improvements may be realized by increasing sintering time so that greater densification occurs before cooling and solidification of the liquid phases. The interactions between the glass additives and the BZT-BT bulk require further study; backscatter electron imaging appeared to indicate the presence of minority phases within the BZT-BT bulk, but these phases were not able to be clearly characterized.

5. DIELECTRIC BEHAVIOR

5.1. GLASS DIELECTRIC PROPERTIES

Dielectric measurements were performed at room temperature on samples of each glass for use in modeling the dielectric constant of BZT-BT dielectrics with residual discontinuous or continuous phases (glassy or crystalline) after liquid phase sintering.

Cylinders of the $30Bi_2O_3$-$30ZnO$-$40B_2O_3$ and $50Bi_2O_3$-$25B_2O_3$-$25SiO_2$ glasses were cast for dielectric measurement. Samples of each glass were melted in alumina crucibles at 950°C for 2-3 hours and cast into 10mm diameter steel cylinder molds. The cylinders were immediately removed once solidified and annealed at 350°C for 30 minutes prior to cooling to room temperature. Both cylinders were transparent, indicating no macroscopically observable recrystallization occurred during cooling and annealing. The cooled cylinders were then cut into 5-8mm thick wafers using a diamond saw lubricated with mineral oil; the top and bottom faces of the cylinders were subsequently polished to a 0.25μm surface finish with SiC and diamond papers and suspensions. The polished surfaces were then electroded with colloidal silver paste (Ted Pella, Inc.). Capacitance and loss tangent measurements were performed an Agilent 4194 Impedance/Gain Phase Analyzer from 100Hz to 100kHz. The dielectric constants of each glass were then calculated from the sample dimensions and capacitance measurements.

Across the selected frequency range, both the $30Bi_2O_3$-$30ZnO$-$40B_2O_3$ and $50Bi_2O_3$-$25B_2O_3$-$25SiO_2$ glasses maintained a frequency-independent dielectric constant of ≈37 and loss tangents below ≈0.005. Kim, *et al.* reported a much lower dielectric constant of 21 for the $30Bi_2O_3$-$30ZnO$-$40B_2O_3$ glass.[25] Huebner and Zhang reported a dielectric constant of 39.5 for the $50Bi_2O_3$-$25B_2O_3$-$25SiO_2$ glass, which agrees well with the value of 37 calculated in this work.[24]

5.2. GLASS-CONTAINING BZT-BT DIELECTRIC PROPERTIES

Dielectric studies were undertaken to assess the electrical performance of the liquid phase sintered components. Of critical importance is the preservation of the relaxor ferroelectric behavior characteristic of pure 20BZT-80BT, with its relatively temperature- and field-stable dielectric constant. Dielectric constant and loss versus temperature, and polarization-electric field measurements were employed to characterize the electrical properties of the liquid phase sintered components relative to pure BZT-BT in terms of dielectric constant and energy storage capability. Attempts to model the dielectric properties were also performed based on the previous analyses of interactions between the liquid phase formers and the BZT-BT bulk.

5.2.1. Dielectric Properties. Pellets sintered with 1, 2, and 5v% additions of either the borate or borosilicate glass were studied to assess the dielectric effects of the liquid phase sintered parts. Samples were prepared using the methods described previously in Section 4.1, and subsequently sintered at 1000°C for 4 hours in 20BZT-80BT sacrificial powder beds under stagnant air and ramp rates of ±5°C/min. The sintering process yielded parts with bulk densities greater than 88% of theoretical for all pellets. The pellets were then polished, coated with sputtered Cr/Au electrodes on the flat surfaces, and subjected to dielectric property tests to measure the temperature dependence of capacitance and loss tangent in a Thermotron environmental chamber using an HP4284A LCR meter with an oscillator magnitude of 1V. Polarization-electric field behavior was measured at 1Hz using a Radiant Technologies Precision Workstation connected to a Trek 10kV amplifier.

All compositions and concentrations retained the relaxor-type behavior exhibited by pure 20BZT-80BT. FIG. 5-1, a representative plot for the 1v% $30Bi_2O_3$-30ZnO-$40B_2O_3$ glass, shows the frequency dispersion and diffuse maxima in dielectric constant and dissipation factor as a function of temperature characteristic of relaxor behavior.

The temperature dependence of the dielectric constant and loss tangent is illustrated in FIG. 5-2 at 1kHz for each glass additive as a function of volume concentration. Additions of the borate glass yielded an expected decrease in dielectric constant with increasing glass concentration, as the lower permittivity glass (and the phases subsequently formed by reaction with the BZT-BT) decreased the overall permittivity of the sample. Additions of the borosilicate decreased the dielectric constant by nearly 40%, with no apparent trend between additive content and K. The loss tangent values associated with each glass composition and concentration were nearly equivalent across all temperatures. Losses for the glass-containing samples were lower than for pure 20BZT-80BT below T_m. At temperatures above T_m (up to a maximum measurement temperature of 180°C), the loss tangent for all samples was less than 0.01.

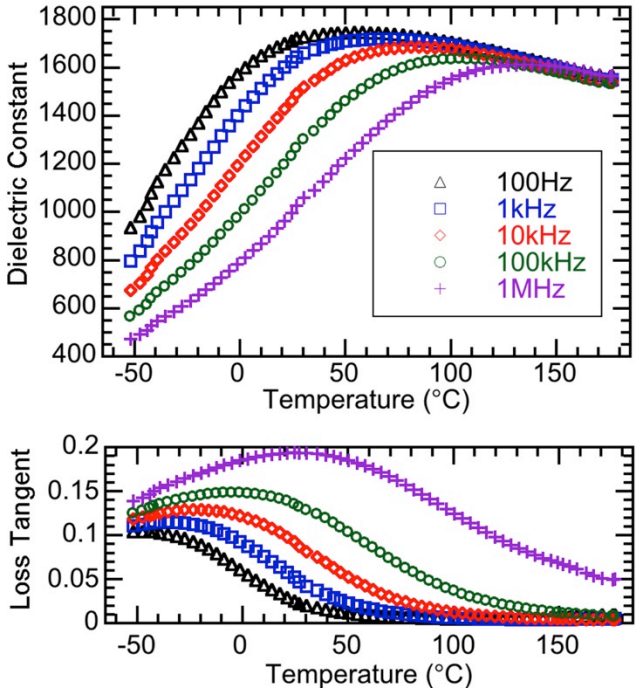

FIG. 5-1. Representative relaxor behavior in dielectric constant/dissipation factor vs. temperature exhibited for all additions of glass compositions/concentrations studied.

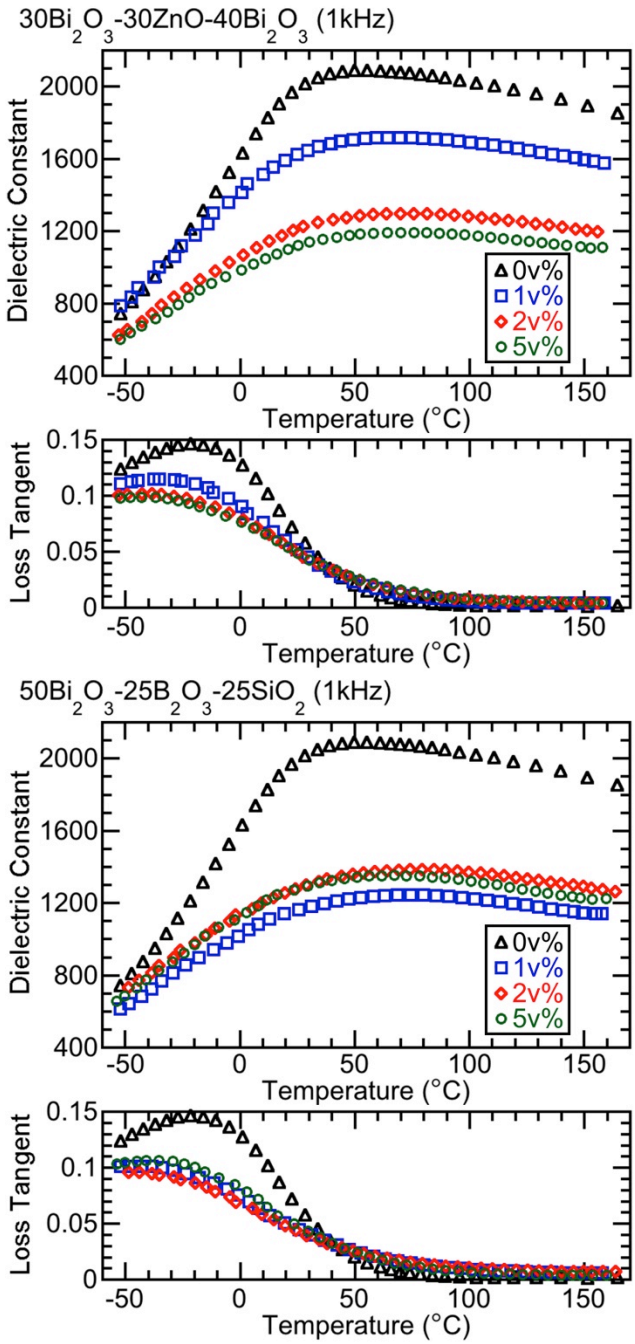

FIG. 5-2. Temperature-dependent permittivity and loss for each glass composition/concentration.

The behavior of the dielectric constant at temperatures above T_m was characterized in terms of the diffuseness of the dielectric constant maximum (δ). The diffuseness was found by

fitting the observed K versus T behavior at 1kHz to the power law relation for relaxor ferroelectrics[32]:

$$\frac{1}{K}=\frac{1}{K_{max}}+\frac{(T-T_m)^{\gamma}}{2K_{max}\delta^{\gamma}} \quad (1 \le \gamma \le 2) \tag{5-1}$$

The exponent γ and diffuseness δ were found using a least squares regression fitting Equation 5-1 to the measured data in terms of 1/K versus $(T-T_m)^{\gamma}$. These fit parameters are shown for pure 20BZT-80BT and each glass composition and concentration in Table 5.1. The magnitude and similarity in the calculated δ values for all compositions ($223 < \delta < 256$) is indicative of the highly diffuse transition, leading to good temperature stability of the dielectric constant at temperatures above T_m (up to ≈ 180°C). At temperatures between T_m and 180°C, K decreased by less than 10% from K_{max} in all cases (including pure 20BZT-80BT).

Table 5.1. Fitted power law parameters γ and δ for each glass composition and concentration.

Composition	T_m (°C)	K_{max}	γ	δ
BZT-BT	54	2090	1.63	256
Borate				
1v%	67	1720	1.69	252
2v%	73	1300	1.64	246
5v%	73	1190	1.64	246
Borosilicate				
1v%	73	1250	1.60	225
2v%	77	1390	1.65	232
5v%	67	1350	1.57	223

The polarization-electric field (P-E) behavior for each of the glass compositions (shown in FIG. 5-3) exhibits the superparaelectric behavior typical of a relaxor ferroelectric. All curves have narrow/closed loops with a ≈0 remanent polarization. In all cases, the curves show that K remains relatively constant at fields as high as 100kV/cm.

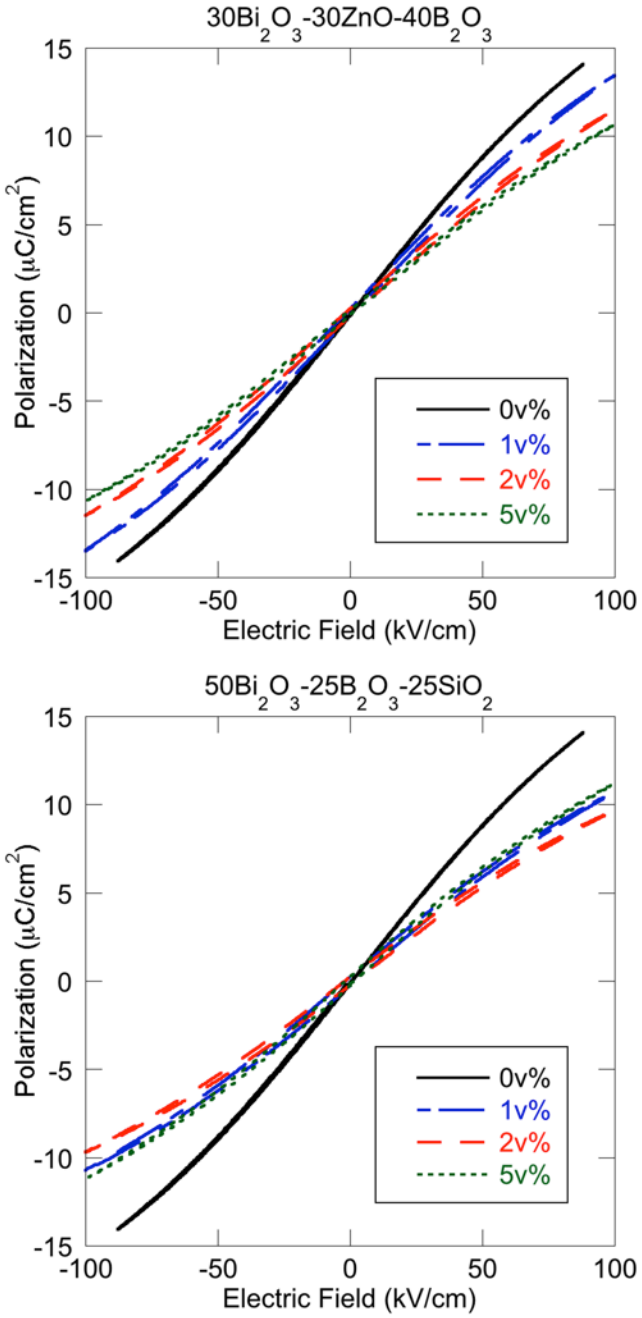

FIG. 5-3. Polarization vs. electric field behavior for each glass composition and concentration.

The field-dependent K, shown in FIG. 5-4, was calculated using linear estimations of the slopes of the P-E curves; these calculations are equivalent to the low-signal K with a DC bias equivalent to the x-axis value. The dielectric constant values for all liquid phase sintered samples

were less than or equal to that of pure 20BZT-80BT. However, K remained above 800 for all borate compositions and above 700 for the borosilicate-containing samples at fields of 100kV/cm.

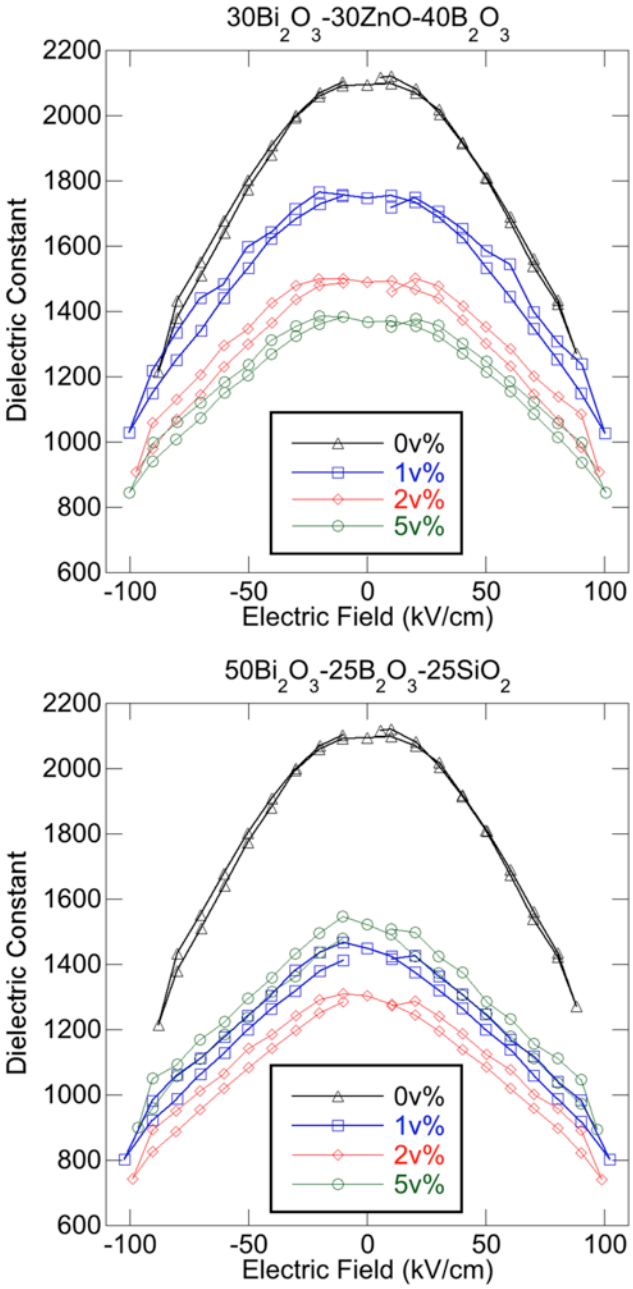

FIG. 5-4. Dielectric constant vs. electric field plots calculated from the polarization-field behavior of each glass composition and concentration.

All samples were able to withstand fields of 100kV/cm without electrical breakdown. As such, estimates of energy density (E_d) of these liquid phase sintered dielectrics were calculated from the dielectric constants at 100kV/cm with Equation 5-2:

$$E_d = \frac{1}{2}\varepsilon_0 K E^2 \qquad (5\text{-}2)$$

The calculated energy densities (at 100kV/cm field strengths) for pure 20BZT-80BT and all glass compositions and concentrations studied are given in Table 5.2. As expected, pure BZT-BT exhibits the highest energy density; however, energy densities above 0.4 J/cm^3 were still exhibited by the dielectrics sintered with borate glass additions, and above 0.3 J/cm^3 for the borosilicate-containing samples at only 100kV/cm fields. Based on the observed K-E behavior, application of modestly higher field strengths (150-200 kV/cm fields) would likely lead to much higher energy densities that approach those of polymer film capacitors (1-2 J/cm^3), while still preserving the high power density typical of ceramic capacitors.[33] This is especially likely for 1v% additions of the $30Bi_2O_3$-30ZnO-$40B_2O_3$ glass, as the dielectric constant of these samples remained above 1000 for the 1v% composition at 100kV/cm field strengths.

Table 5.2. Energy density estimates for 20BZT-80BT dielectrics with liquid phase sintering additives.

Composition	E_d (J/cm^3)
BZT-BT	0.6
Borate	
1v%	0.5
2v%	0.4
5v%	0.4
Borosilicate	
1v%	0.4
2v%	0.3
5v%	0.4

5.2.2. Dielectric Modeling. X-ray diffraction studies were performed on the liquid phase sintered samples of each composition and concentration in an attempt to characterize the phases contributing to the observed dielectric behavior. Post-sintering XRD patterns were inconclusive for minority phase identification; representative XRD plots for samples with 5v% glass additions, shown in FIG. 5-5, showed only peaks corresponding to the cubic $BaTiO_3$ structure.

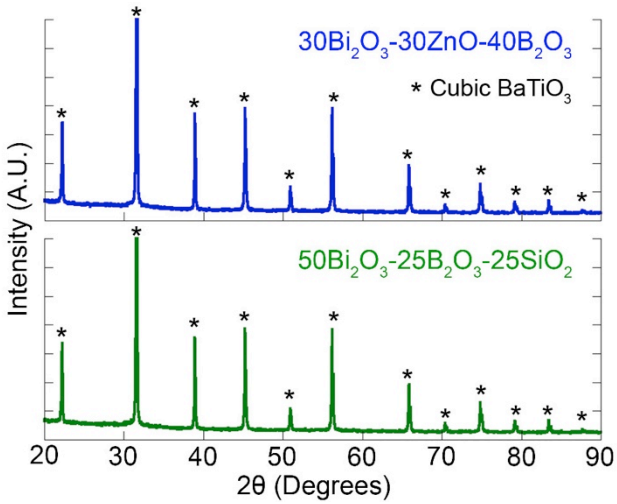

FIG. 5-5. X-ray diffraction plots from crushed pellets containing 5v% of each glass and sintered at 1000°C.

Previous study of the macroscopic interfaces between these glasses and BZT-BT described in Section 3.3.2 suggested that the borate glass reacted with BZT-BT to form Aurivillius-type bismuth titanate (such as $Bi_4Ti_3O_{12}$, BiT) or barium bismuth titanate phases detectable by backscatter SEM and XRD. The borosilicate glass appeared to form a crystalline silicate phase (possibly $BaSiO_3$, Ba_2SiO_4, or Ba_2SiO_5) when in contact with BZT-BT.

Based on these observations, some initial attempts to model the observed dielectric behavior were undertaken. The Lichtenecker model for discontinuous second phases in a continuous primary phase is a simple starting point and a test to see if the measured dielectric

performance can be described by the presence of discontinuous glassy or crystalline phase within the BZT-BT bulk.

The Lichtenecker equation for a two-phase system is:

$$\ln(K') = V_1 \ln(K_1) + V_2 \ln(K_2) \quad (5\text{-}3)$$

where K' = the effective dielectric constant of the multiphase material,

V_1 = volume fraction of Phase 1

K_1 = dielectric constant of Phase 1

V_2 = volume fraction of Phase 2

K_2 = volume fraction of Phase 2.

For simplicity, the discontinuous second phase is assumed to be either glass, or all crystalline, such as $Bi_4Ti_3O_{12}$ (K = 100)[34] for the borate-containing samples or $BaSiO_3$ (K = 7.9, calculated with the Clausius-Mosotti relationship for orthorhombic $BaSiO_3$) for the borosilicate-containing samples. The dielectric constants for the glasses and pure 20BZT-80BT were measured as follows at ~21°C and 1kHz: $K_{BZT\text{-}BT} = 1953$; $K_{30Bi2O3\text{-}30ZnO\text{-}40B2O3} = 37$; and $K_{50Bi2O3\text{-}30ZnO\text{-}35B2O3} = 37$.

Using these values, the volume fractions of discontinuous glass or crystalline phase necessary to give the observed dielectric properties at ~21°C are given in Table 5.3. In all cases, the calculated volume fractions are significantly greater than the volume fraction of glass added as sintering aids. Dissolution of BZT-BT grains during reaction with the glasses may account for the greater fractions of second phases from the calculations.

Table 5.3. Amounts of glassy/crystalline second phase expected from Lichtenecker model calculations.

Composition	K	$V_{Glass\ Only}$	$V_{Xtal\ Only}$
Borate			
1v%	1600	5%	7%
2v%	1190	13%	17%
5v%	1100	15%	19%
Borosilicate			
1v%	1150	13%	10%
2v%	1270	11%	8%
5v%	1270	11%	8%

Modeling was also attempted using brick wall-style calculations developed by Frey and Payne for continuous second phases and continuous grain boundary regions of different permittivities.[5] The volume fractions and thicknesses of continuous glass and crystalline phase necessary to generate the observed dielectric properties were calculated using the following equations:

$$\frac{1}{K'} = \frac{V_1}{K_1} + \frac{gV_2}{K_2} \qquad (5\text{-}4)$$

where K' = dielectric constant of the multiphase material

K_1 = dielectric constant of the bulk phase

V_1 = volume fraction of the bulk phase

K_2 = dielectric constant of the continuous second phase

V_2 = volume fraction of the continuous second phase

g = geometric factor, equal to the fraction of the second phase interrupting electric field passage.

Values of g are dependent on the bulk phase grain geometry. Spherical grains correspond to $g \approx 1$, but a value of $g = 0.8$ was obtained for $BaTiO_3$-based dielectrics by Payne and Cross.[5]

The volume fractions of each phase can be calculated from measurements of grain size and second phase thickness as follows:

$$V_1 = \left(1 + \frac{d_2}{d_1}\right)^{-3} \quad (5\text{-}5)$$

and

$$V_2 = 1 - V_1 \quad (5\text{-}6)$$

where d_1 = width of the bulk phase grains (μm)

d_2 = thickness of the second phase layer (μm)

Using these equations, the second phase volume fraction (V_2) and second phase thickness (d_2) of glass and BiT/$BaSiO_3$ corresponding to the observed dielectric constant values were calculated; the results are shown in Table 5.4. SEM measurements on the sintered glass-containing parts indicated an average grain size of approximately 750 nm, and a value of g = 0.8 was assumed.

Table 5.4. Brick wall model calculations of second phase volume fraction and thickness.

Composition	K	Glass Only		Crystal Only	
		V_2 (%)	d_2 (nm)	V_2 (%)	d_2 (nm)
Borate					
1v%	1600	0.5	1	1.5	4
2v%	1190	1.6	4	4.4	11
5v%	1100	1.9	5	5.3	14
Borosilicate					
1v%	1150	1.7	4	0.4	1
2v%	1270	1.3	3	0.3	1
5v%	1270	1.3	3	0.3	1

The brick wall model perhaps offers more reasonable second phase volume fractions than the Lichtenecker model calculations, but neither model clearly matches up with the volume fractions of glass used as liquid phase sintering aids. The validity of these volume fractions and thicknesses cannot be confirmed directly due to limited understanding of the reactions, volume changes, and phase formation associated with the borate/BZT-BT interactions during sintering. Further study utilizing transmission electron microscopy is needed to characterize the presence, if any, of a continuous grain boundary phase/region as a function of initial glass concentration.

5.2.3. Summary. Samples sintered with additions of ≤5v% $30Bi_2O_3$-30ZnO-$40B_2O_3$ or $50Bi_2O_3$-$25B_2O_3$-$25SiO_2$ retained the relaxor behavior characteristic of the host BZT-BT, and exhibited reduced dielectric constants relative to the pure material. All samples also exhibited high dielectric constants (>700) under applied electric fields of 100kV/cm, suggesting that these samples would make useful high energy density dielectrics when subjected to 150-200 kV/cm fields. Simple dielectric modeling using the Lichtenecker and brick wall models did not directly explain the dielectric performance characteristics observed based on the observed phases formed alone.

6. CONCLUSIONS AND FUTURE WORK

6.1. CONCLUSIONS

The results of the studies detailed in this thesis indicated that reductions in the sintering temperature of 20BZT-80BT dielectrics could be realized through additions of both the $30Bi_2O_3$-$30ZnO$-$40B_2O_3$ and $50Bi_2O_3$-$25B_2O_3$-$25SiO_2$ (mol%) glasses. Samples produced with 1v% borate additions and 5v% additions of either the borate or borosilicate reached relative densities in excess of 95% after sintering at 1000°C for four hours, versus 90% relative density for pure BZT-BT sintered under the same conditions. Higher densities can likely be achieved through optimization of the sintering time/rate at 1000°C, thus allowing these liquid phase sintered dielectrics to be produced at temperatures 180°C lower than the 1180°C used currently for pure BZT-BT.

Additions of the liquid phase sintering aids were accompanied by reductions in the dielectric constant as a function of temperature and electric field. The reduction in K increased with increasing glass concentration for the borate glass, whereas additions of the borosilicate glass yielded no clear trend in dielectric constant as a function of volume concentration. All samples, however, retained the relaxor behavior of the 20BZT-80BT bulk in the form of large, diffuse maxima as a function of temperature, and narrow polarization-electric field loops at field strengths as high as 100kV/cm.

The energy densities of the liquid phase sintered dielectrics were estimated to be between 0.3-0.5 J/cm^3 for all glass compositions and concentrations. Higher energy densities were achieved by samples with lower glass additions. Of particular interest are dielectrics with 1v% $30Bi_2O_3$-$30ZnO$-$40B_2O_3$; samples of this composition achieved relative densities of 96% and energy densities of ≈0.5 J/cm^3 under electric field strengths of 100kV/cm. The high sintered density of these dielectrics should allow application of higher fields in the range of 150-

200kV/cm, but could not be tested due to limitations in the electrical testing equipment. Increasing in the electric field strength should boost the energy density of these dielectrics into the polymer film capacitor range, while maintaining the high power density of ceramic dielectrics. These dielectrics thus show promise for high field, high energy density capacitor applications.

Study of macroscopic interfaces between BZT-BT and each of the glass additives indicated that thin layers (≤10μm) of crystalline phases formed along the interface. An Aurivillius-type bismuth titanate phase (suspected to be $Bi_4Ti_3O_{12}$) crystallized during reaction between the borate glass and a BZT-BT surface after processing at 700°C. This phase was likely formed through diffusion of Ti from the BZT-BT grains into the surrounding borate glass. A barium silicate phase (likely $BaSiO_3$) crystallized at the borosilicate/BZT-BT interface after processing at 800°C, requiring diffusion of Ba out of the BZT-BT and into the glass. Similar phases are expected to be present in the BZT-BT dielectrics sintered with additions these glasses, but these phases were not definitively detected and characterized in this study.

6.2. FUTURE WORK

A number of important topics and questions developed over the course of this research remain unanswered and warrant further study, including:

- *TEM study of grain boundaries in liquid phase sintered dielectrics* – Since the presence and composition of secondary phases in the grain boundaries of liquid phase sintered BZT-BT were not easily characterized, transmission electron microscopy is necessary to gain an accurate understanding of the identity and distribution of second phases within the grain boundaries and along grain surfaces for purposes of dielectric modeling.
- *Development of a $Bi(Zn_{0.5}Ti_{0.5})O_3$-$BaTiO_3$ phase diagram* – No phase diagram currently exists for the BZT-BT binary system. Development of such a diagram would be useful in

understanding the role of Bi excess or deficiency in BZT-BT formation, electrical properties, and sintering behavior.

- *Sintering time/heating rate optimization* – In these sintering studies, the sintering temperature was varied while fixing the sintering time (4 hours) and heating rate (5°C/min). Study of the effects of sintering time and heating rate on densification could yield dense liquid phase sintered dielectrics at temperatures below 1000°C.
- *High electric field breakdown strength testing* – In general, application of 100kV/cm electric fields was the highest achievable field strength due to equipment characteristics and sample thicknesses. Preparation of dense liquid phase sintered samples for statistical breakdown strength testing would be useful in determining the maximum sustainable electric field strengths for the liquid phase sintered dielectrics. Knowledge of these maximum fields, in turn, would allow better estimation of the highest possible energy densities for these dielectrics.

APPENDIX: $35Bi_2O_3$-30ZnO-$35B_2O_3$ STUDY

Studies began on the use of a second bismuth-zinc-borate glass composition, $35Bi_2O_3$-30ZnO-$35B_2O_3$ (mol%), as a sintering aid for BZT-BT. This glass composition was subjected to a subset of the analyses performed on the $30Bi_2O_3$-30ZnO-$40B_2O_3$ and $50Bi_2O_3$-$25B_2O_3$-$25SiO_2$ glasses.

A.1. GLASS FORMULATION

The $35Bi_2O_3$-30ZnO-$35B_2O_3$ glass was formulated and processed in the same manner as the $30Bi_2O_3$-30ZnO-$40B_2O_3$ and $50Bi_2O_3$-$25B_2O_3$-$25SiO_2$ glasses described in Section 3.1. The glass was fabricated by stoichiometric mixing and melting of Bi_2O_3, ZnO, and B_2O_3 (≥99.0%, Alfa-Aesar) in a covered alumina crucible at 950°C for three hours. Samples for capacitance and loss tangent measurements were made by casting molten glass into 10mm diameter steel cylinder molds and annealing at 350°C for 30 minutes before cooling to room temperature. The remaining glass was quenched between copper plates. Both the annealed cylinders and quenched glass were transparent, indicating that no macroscopically observable crystallization occurred on cooling.

In preparation for distribution of the glass within the 20BZT-80BT, the quenched glass was crushed with a mortar and pestle. The resultant powders were then ball milled for 24 hours and attrition milled for 2 hours with stabilized ZrO_2 media in ethanol. Dynamic light scattering (Zetasizer, Malvern Instruments) particle size measurements indicated the milled glass particles were larger than desired (≥800nm). Gravitational sedimentation was subsequently employed to extract glass particles with diameters smaller than 800nm. Small amounts of the glass powder (<10g) were dispersed in ethanol with 1wt% polyvinylpyrrolidone and added to the top of a sedimentation cone filled with ethanol. After allowing time for particles larger than 800nm to settle out (several hours for >10cm sedimentation height, calculated via Stokes' Law), the

supernatant was removed with a syringe and subjected to dynamic light scattering analysis. DLS measurements indicated the average diameter of glass particles in the supernatant was <600nm. The supernatant was then dried to allow extraction of the glass particles.

A.2. THERMAL CHARACTERIZATION

Differential thermal analysis and *in situ* wetting angle observations were again employed in an abbreviated study of the thermal behavior of the $35Bi_2O_3$-30ZnO-$35B_2O_3$ glass itself and the interactions between the glass and 20BZT-80BT. The glass DTA scan and wetting behavior on heating of this glass were similar to the behavior of the previously studied $30Bi_2O_3$-30ZnO-$40B_2O_3$ composition, suggesting that many of the interactions between the BZT-BT and the $30Bi_2O_3$-30ZnO-$40B_2O_3$ glass would be similar for this glass composition.

A.2.1. Glass Differential Thermal Analysis. DTA was again used to measure the glass transition temperature (T_g), melting temperature (T_{melt}) and any crystallization temperatures (T_x) on heating of the $35Bi_2O_3$-30ZnO-$35B_2O_3$. These temperatures were used as initial indicators of the viability of the glass as a sintering aid for BZT-BT. A powder sample of the glass fabricated in Section A.1 was subjected to differential thermal analysis in a Netzsch STA409 DTA. The sample was placed in an alumina crucible and heated in air to 800°C at a rate of 5°C/min. (As mentioned in Section 3.2, analysis temperatures were limited to 800°C to prevent damage to the DTA.)

FIG. A-1 shows the DTA curve for the $35Bi_2O_3$-30ZnO-$35B_2O_3$ glass, along with the curve for the $30Bi_2O_3$-30ZnO-$40B_2O_3$ glass for comparison. The $35Bi_2O_3$-30ZnO-$35B_2O_3$ glass showed a sharp crystallization exotherm and melting endotherm below 800°C. T_g was believed to be around 385°C, which was lower than the 418°C observed for the compositionally similar $30Bi_2O_3$-30ZnO-$40B_2O_3$ glass. A crystallization event occurred at 550°C, nearly 70°C lower than the T_x observed for the $30Bi_2O_3$-30ZnO-$40B_2O_3$ glass. Melting of the crystalline phase occurred

just below the melting temperature of the crystals formed from the $30Bi_2O_3$-$30ZnO$-$40B_2O_3$ glass (675°C).

Both borate glass compositions lie within the $Zn_3B_2O_6$-$ZnBi_4B_2O_{10}$-$Bi_3Bi_5O_{12}$ phase field on the Bi_2O_3-ZnO-B_2O_3 ternary phase diagram (shown previously in FIG. 3-4), again suggesting that a mixture of the three phase field components formed at the observed T_x of 550°C. As before, a more in-depth investigation into these recrystallized phases was not performed. The effect of glass particle size on crystallization behavior was also not investigated.

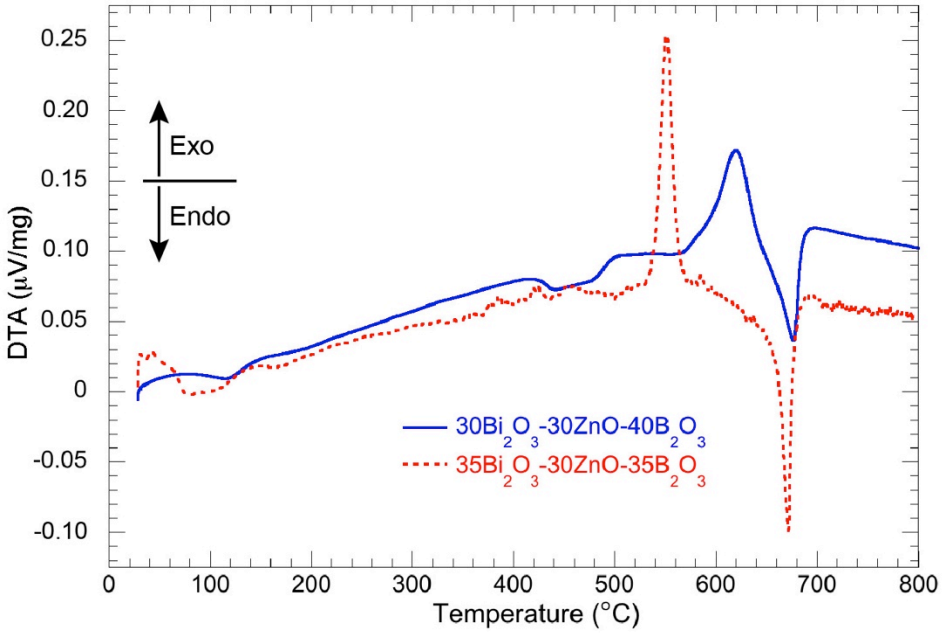

FIG. A-1. DTA curves for both borate glasses on heating in air to 800°C at 5°C/min.

A.2.2. *In Situ* Wetting Angles. The wetting behavior of the $35Bi_2O_3$-$30ZnO$-$35B_2O_3$ glass was observed *in situ* with optical photography in the manner previously described in Section 3.3.A. A small piece (approximately 2mm on a side) of glass was placed on top of a sintered 20BZT-80BT pellet in a tube furnace and heated at 3°C/min to 700°C. The sample was

photographed at regular intervals during heating, and the corresponding sample temperature was measured with a Type K thermocouple placed next to the sample.

Photographs showing the change in shape of the $35Bi_2O_3$-30ZnO-$35B_2O_3$ glass during heating are shown in FIG. A-2. No shape changes occurred on heating to 410°C, but between 410°C and 500°C, the glass softened, allowing surface tension to reshape the glass into a droplet. The droplet spread during heating to 675°C. Between 675°C and 700°C, the glass reached the melting temperature indicated via DTA, and the glass completely covered the pellet surface and sides. Complete wetting of the BZT-BT at/below 700°C confirms that the $35Bi_2O_3$-30ZnO-$35B_2O_3$ could also be a viable sintering aid candidate for BZT-BT.

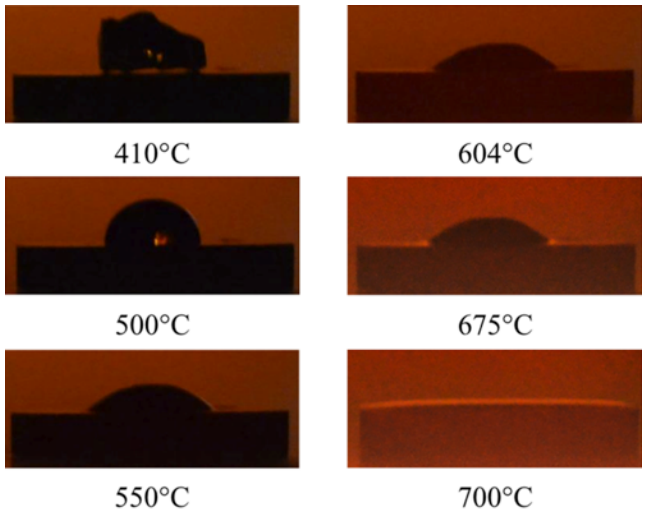

FIG. A-2. Photograph series showing wetting behavior of the $35Bi_2O_3$-30ZnO-$35B_2O_3$ glass in contact with 20BZT-80BT during heating to 700°C.

The sample used for *in situ* wetting angle observations was destroyed during attempts to remove it from the alumina tube, as the $35Bi_2O_3$-30ZnO-$35B_2O_3$ glass had fused the sample to the alumina surface so well that the sample fractured into multiple small pieces during removal. As

such, *ex situ* interface observations were not performed for the $35Bi_2O_3$-30ZnO-$35B_2O_3$ glass/BZT-BT interface. Based on the compositional similarity between the $35Bi_2O_3$-30ZnO-$35B_2O_3$ and the previously examined $30Bi_2O_3$-30ZnO-$40B_2O_3$ glass, the formation of a similar interfacial crystallization layer of $Bi_4Ti_3O_{12}$ was expected to occur during heating and cooling of the $35Bi_2O_3$-30ZnO-$35B_2O_3$/BZT-BT sample (see Section 3.3.2).

A.3. GLASS/BZT-BT DENSITIES AND MICROSTRUCTURES

Half-inch diameter pellets of 20BZT-80BT containing 1, 2, and 5v% $35Bi_2O_3$-30ZnO-$35B_2O_3$ glass were prepared by the same processes outlined in Section 4.1. Three pellets of each concentration were sintered in 20BZT-80BT sacrificial powder beds at 950°C and 1000°C for four hours with a heating rate of 5°C/min, based on previous work with the other glass compositions that indicated that 1000°C was a useful sintering temperature. The bulk densities of the pellets were again measured by the Archimedes method in kerosene.

The bulk densities of the $35Bi_2O_3$-30ZnO-$35B_2O_3$-containing pellets sintered at 950°C and 1000°C are shown in FIG. A-3. All volume concentrations of the $35Bi_2O_3$-30ZnO-$35B_2O_3$ yielded sample densities above the 90% relative density of the pure 20BZT-80BT sintered at 1000°C for four hours. Of particular interest is the 1v% $35Bi_2O_3$-30ZnO-$35B_2O_3$ composition, due to its high density (>95%) and minimum level of additional phases that would likely reduce the dielectric constant of the 20BZT-80BT.

Due to compositional similarity with the $30Bi_2O_3$-30ZnO-$40B_2O_3$ glass, the formation of a bismuth titanate-type crystalline phase was expected at the interfaces between the $35Bi_2O_3$-30ZnO-$35B_2O_3$ glass and BZT-BT grains. This crystalline phase would likely have melted below 1000°C, as detailed previously in Section 4.1; melting of the crystalline phase would enhance the densification of the BZT-BT dielectric by either removing barriers to matter transport or by simply contributing additional liquid phase to the sintering process. As such, the high sample

densities after sintering at 1000°C for four hours matched well with previous results for the borate-containing samples.

As with the $30Bi_2O_3$-30ZnO-$40B_2O_3$- and $50Bi_2O_3$-$25B_2O_3$-$25SiO_2$-containing samples, pellets containing 2v% of each glass were the least dense of any of three glass concentrations. This trend was, as before, possibly the consequence of the 5v% composition lying in a different phase field on the BZT-BT + Bi-Zn-borate phase diagram. Since no such phase diagram exists, however, this explanation cannot be confirmed.

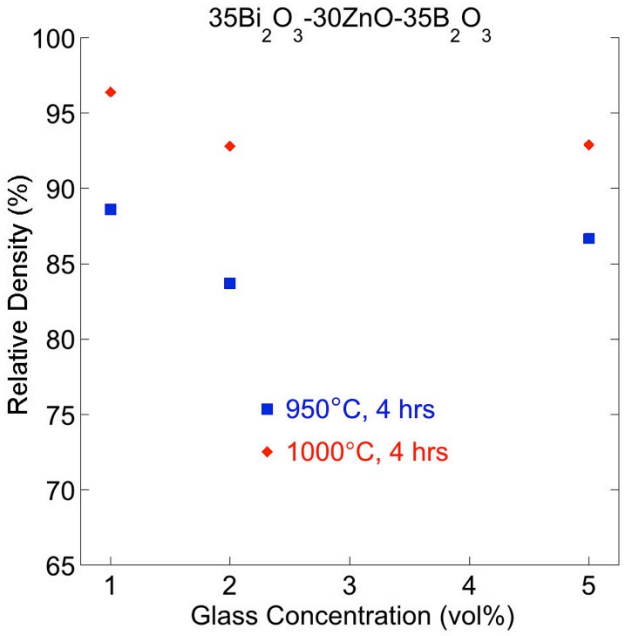

FIG. A-3. Bulk densities of $35Bi_2O_3$-30ZnO-$35B_2O_3$-containing pellets after sintering at 950°C and 1000°C for four hours.

Microstructural imaging of the sample containing 5v% glass after sintering at 1000°C was performed with secondary and backscatter electron imaging, as shown in FIG. A-4. As with the samples containing 5v% $30Bi_2O_3$-30ZnO-$40B_2O_3$, the sintered parts appeared to be dense,

though the occasional pore or grain pullout site can also be observed (FIG. A-4a). Backscatter electron imaging (FIG. A-4b) shows the typical mottled grain contrast characteristic of 20BZT-80BT, along with high-Z (bright) regions attributed to the expected BiT second phase.

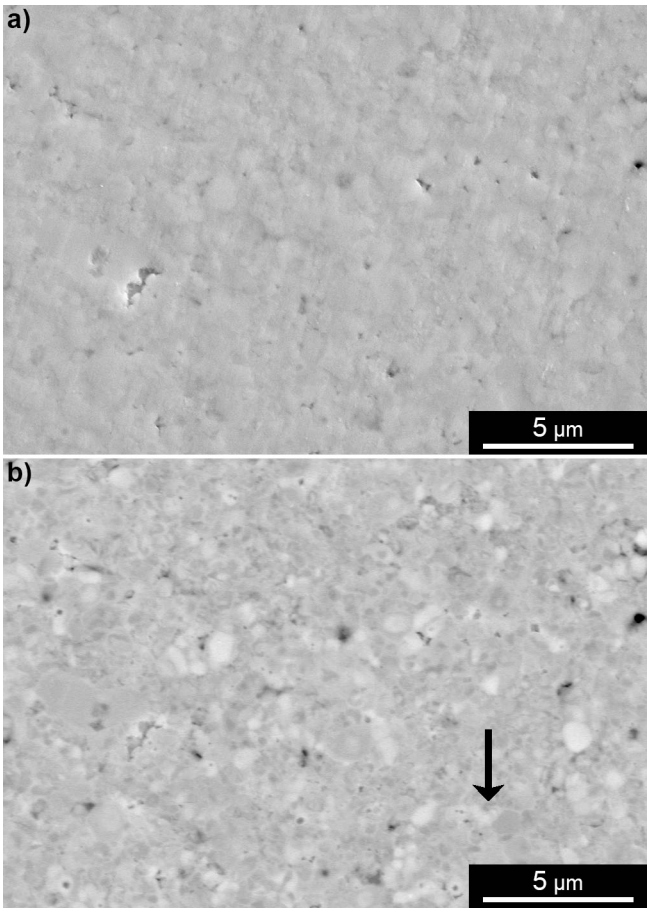

FIG. A-4. (a) Secondary and (b) backscatter electron imaging of a 20BZT-80BT sample containing 5v% $35Bi_2O_3$-30ZnO-$35B_2O_3$ sintered at 1000°C for four hours.

Secondary phases were not detected by x-ray diffraction studies (Philips PANalytical X'Pert Pro). The XRD pattern for the 5v% glass sample, shown in FIG. A-5, showed only peaks corresponding to the cubic perovskite structure.

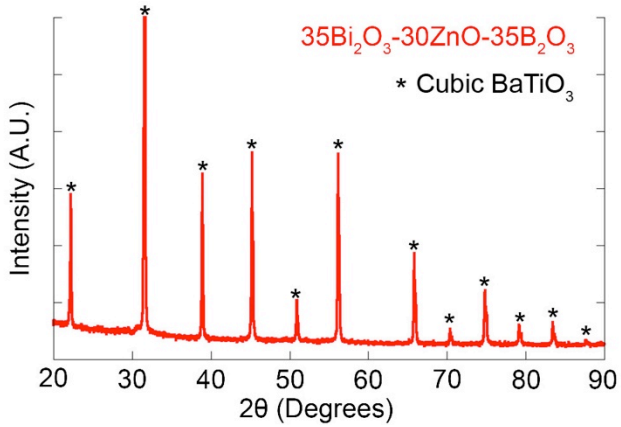

FIG. A-5. Cubic perovskite XRD pattern of 20BZT-80BT + 5v% $35Bi_2O_3$-30ZnO-$35B_2O_3$

A.4. DIELECTRIC CHARACTERIZATION

The BZT-BT dielectrics sintered with additions of the $35Bi_2O_3$-30ZnO-$35B_2O_3$ glass were expected to make useful high energy density dielectrics, since sintering at 1000°C for four hours yielded dielectrics with ≥93% relative densities. Based on similar results for BZT-BT sintered with the $30Bi_2O_3$-30ZnO-$40B_2O_3$ and borosilicate glasses, these dielectrics were expected to operate at electric field strengths of 100kV/cm or higher.

A.4.1. Glass Dielectric Properties. The dielectric properties of the base glass were characterized for use during dielectric modeling calculations. A transparent 10mm cast cylinder of $35Bi_2O_3$-30ZnO-$35B_2O_3$ glass was cut with a diamond saw and polished to a 0.25μm surface finish using SiC paper and diamond suspensions. Colloidal silver electrode paste (Ted Pella, Inc.) was brushed onto the disk faces prior to measurement. Capacitance and loss tangent values were measured with an Agilent 4194 Impedance/Gain Phase Analyzer from 100Hz to 100kHz. The dielectric constant was then calculated from the sample dimensions and capacitance measurements.

The $35Bi_2O_3$-30ZnO-$35B_2O_3$ dielectric constant and loss tangent was nearly frequency-independent over the measured frequency range. A dielectric constant of 30 was calculated for

the glass, while the loss tangent was measured below 0.002. This value is lower than the dielectric constant calculated for the $30Bi_2O_3$-30ZnO-$40B_2O_3$ glass (K = 37), but is closer to the K values reported for similar glasses in the Bi_2O_3-ZnO-B_2O_3 system by Kim, *et al*.[25]

A.4.2. BZT-BT/Glass Dielectric Behavior. Pellets sintered at 1000°C for four hours with 1,2, and 5v% $35Bi_2O_3$-30ZnO-$35B_2O_3$ additions were polished, coated with sputtered Cr/Au electrodes on the flat surfaces, and subjected to dielectric measurements in the manner described in Section 5.2.1. The temperature-dependent capacitance and dissipation factor were measured in a Thermotron environmental chamber using an HP4284A LCR meter with a 1V oscillator magnitude. Polarization-electric field behavior was measured at a frequency of 1Hz using a Radiant Technologies Precision Workstation connected to a Trek 10kV amplifier.

Dielectric constant and loss tangent values for the 1, 2, and 5v% $35Bi_2O_3$-30ZnO-$35B_2O_3$ glass concentrations measured at 1kHz from -55°C to 170°C are shown in FIG. A-6.

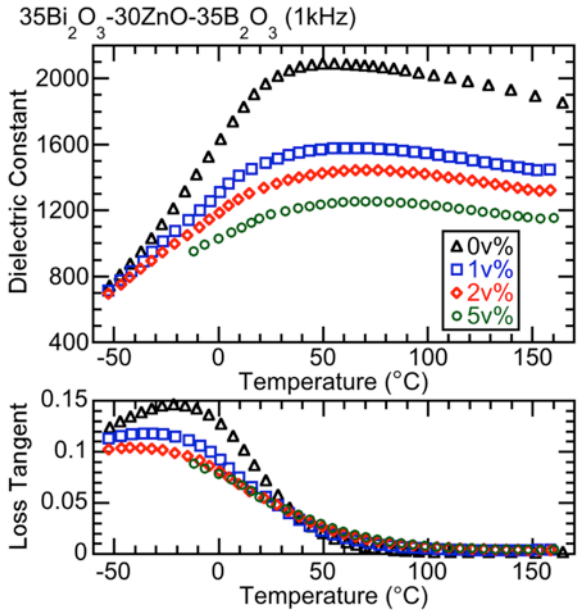

FIG. A-6. Dielectric constant/loss tangent measurements as a function of temperature for 1, 2, and 5v% additions of $35Bi_2O_3$-30ZnO-$35B_2O_3$ glass.

The diffuse dielectric constant maximum typical of relaxor behavior was again observed for samples containing all concentrations of the glass. As with the $30Bi_2O_3$-30ZnO-$40B_2O_3$ glass, increasing additions of the $35Bi_2O_3$-30ZnO-$35B_2O_3$ led to larger reductions in dielectric constant. Above T_m, the loss tangent values were again below 0.01.

The diffuseness of the dielectric constant maximum (δ) was calculated by performing a least squares regression fitting the measured 1kHz data in terms of 1/K versus $(T-T_m)^\gamma$ to the relaxor power relation detailed by Uchino and Nomura:[32]

$$\frac{1}{K}=\frac{1}{K_{max}}+\frac{(T-T_m)^\gamma}{2K_{max}\delta^\gamma} \quad (1 \le \gamma \le 2) \qquad \text{(A-1)}$$

The fit parameters γ and δ are listed in Table A.1 for 20BZT-80BT sintered with no glass, and 1, 2, and 5v% additions of the $35Bi_2O_3$-30ZnO-$35B_2O_3$ glass. The similarity of the γ and δ values between the glass-containing samples, the pure 20BZT-80BT, and the $30Bi_2O_3$-30ZnO-$40B_2O_3$- and borosilicate-containing samples studied in Section 5.2.1 showed that the additions of the glass (and whatever phases form through glass-BZT-BT reactions during sintering) merely decreased the dielectric constant values without altering the relaxor behavior of the BZT-BT. The large values of δ (227-256) indicated that the dielectric constant maximum was highly diffuse, leading to good temperature stability of K between T_m and 170°C.

Table A.1. Fitted parameters γ and δ for each glass concentration.

Composition	T_m (°C)	K_{max}	γ	δ
BZT-BT	54	2090	1.63	256
35-30-35				
1v%	63	1580	1.66	241
2v%	70	1440	1.59	233
5v%	72	1250	1.61	227

The polarization-field behavior for all concentrations of the $35Bi_2O_3$-30ZnO-$35B_2O_3$ glass is shown in FIG. A-7. The loops for samples containing 1 and 2v% glass exhibited near-zero remanent polarizations, whereas the 5v% sample loop captured some loss area. The curve slopes for all samples are less than the pure 20BZT-80BT, reflecting the lower dielectric constants of the glass-containing samples. Minimal saturation occurred up to 90-100kV/cm.

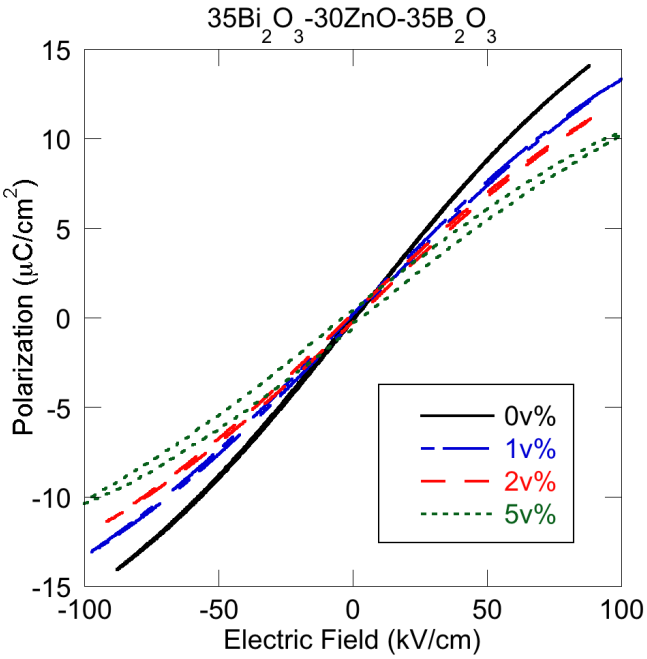

FIG. A-7. Polarization-electric field curves for BZT-BT samples containing 1, 2, and 5v% $35Bi_2O_3$-30ZnO-$35B_2O_3$ glass.

The field dependence of the dielectric constant was calculated as a function of electric field strength using linear estimations of the local P-E curve slopes. These K versus E curves, shown in FIG. A-8, were similar in shape to the K-E curves calculated in Section 5.2.1 for samples containing the $30Bi_2O_3$-30ZnO-$40B_2O_3$ and $50Bi_2O_3$-$25B_2O_3$-$25SiO_2$ glasses. As before,

the dielectric constant values of the glass-containing parts were below those of the pure BZT-BT. The 1 and 2v% compositions maintained K values above 1000 up to 90kV/cm field strengths.

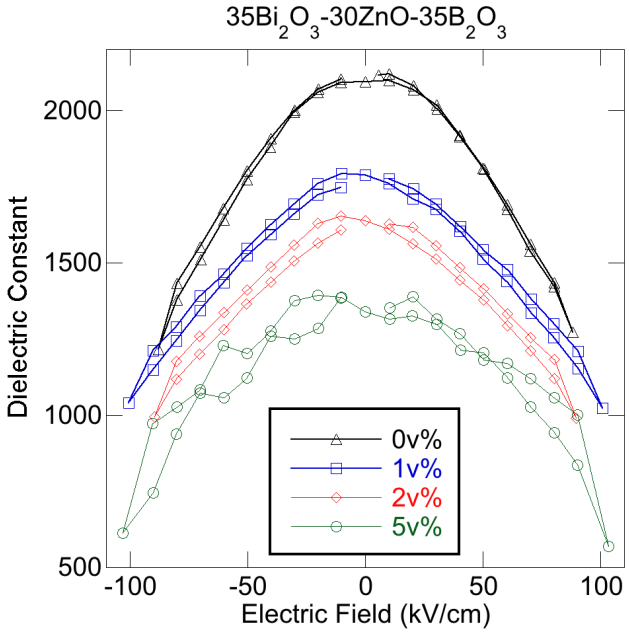

FIG. A-8. Electric field-dependent dielectric constant values of 20BZT-80BT samples containing 1, 2, and 5v% $35Bi_2O_3$-30ZnO-$35B_2O_3$.

The energy densities of these liquid phase sintered dielectrics were again estimated and compared to pure BZT-BT for applied fields of 100kV/cm using Equation (A-2):

$$E_d = \frac{1}{2}\varepsilon_0 K E^2 \qquad \text{(A-2)}$$

The estimated energy densities for the $35Bi_2O_3$-30ZnO-$35B_2O_3$-containing dielectrics are listed in Table A.2. As expected, the pure BZT-BT dielectrics exhibited the highest energy density, but all of the liquid phase sintered dielectrics maintained energy densities above 0.3 J/cm^3. Of particular interest is the 1v% glass composition, which reached nearly full density after sintering at 1000°C for four hours while also having an energy density of 0.5 J/cm^3 at 100kV/cm field strengths. As

with dielectrics sintered with the other glass compositions, increasing the field strength to 150-200kV/cm would likely boost the energy densities of these dielectrics into the polymer film capacitor range, while maintaining the high power density of ceramic capacitors (see Section 5.2.1). BZT-BT dielectrics sintered with ≤5v% additions of $35Bi_2O_3$-30ZnO-$35B_2O_3$ are thus believed to be viable candidates for high field and high energy density capacitor applications.

Table A.2. Energy density estimations for BZT-BT dielectrics sintered with $35Bi_2O_3$-30ZnO-$35B_2O_3$ additions.

Composition	E_d (J/cm^3)
BZT-BT	0.6
35-30-35	
1v%	0.5
2v%	0.4
5v%	0.3

A.4.3. BZT-BT/Glass Dielectric Modeling. Dielectric modeling was performed for BZT-BT sintered with additions of the $35Bi_2O_3$-30ZnO-$35B_2O_3$ glass using the Lichtenecker model for discontinuous second phases and the brick wall model developed for continuous grain boundary phases. The amounts of second phase required to generate the observed dielectric properties at room temperature were calculated using the processes outlined previously in Section 5.2.2. For simplicity, the second phase was assumed to be either all glass (K = 30) or all crystalline $Bi_4Ti_3O_{12}$ (K = 100).[34]

The discontinuous second phase amounts calculated from the Lichtenecker model are listed in Table A.3. The trend of increasing second phase amounts matched the trend of increasing glass additions, but the amounts of second phase were significantly higher than the amounts of glass actually added to the BZT-BT as a sintering aid. The elevated second phase

concentrations could be explained by the glass dissolving some amount of the BZT-BT during sintering, but, as before, this explanation cannot be confirmed from the present results alone.

Table A.3. Discontinuous glassy/crystalline second phase volume fractions expected from Lichtenecker model calculations.

Composition	K	$V_{Glass\ Only}$	$V_{Xtal\ Only}$
35-30-35			
1v%	1480	7%	9%
2v%	1340	9%	13%
5v%	1150	13%	18%

The second phase volume fraction and layer thicknesses calculated with the brick wall model for continuous grain boundary phases are given in Table A.4. As with the Lichtenecker model calculations, the trend of increasing expected second phase volume fraction followed the general increase in glass additions prior to sintering, but does not directly match the amounts of glass added as a sintering aid.

Table A.4. Expected continuous glassy/crystalline second phase fractions and thicknesses calculated with the brick wall model.

Composition	K	Glass Only		Crystal Only	
		V_2 (%)	d_2 (nm)	V_2 (%)	d_2 (nm)
35-30-35					
1v%	1480	0.6	2	2.2	6
2v%	1340	0.9	2	3.2	8
5v%	1150	1.4	3	4.8	12

Given that neither the Lichtenecker nor brick wall model second phase amounts correlated directly with the amount of $35Bi_2O_3$-30ZnO-$35B_2O_3$ glass added to the BZT-BT prior

to sintering, some additional study is needed to experimentally characterize the second phase amounts and distributions in the sintered dielectrics. TEM analysis is ideally suited for determining if a continuous second phase resides in the grain boundaries, and, if so, for characterizing the second phase composition and thickness.

A.5. SUMMARY

Although dielectric modeling was inconclusive in terms of accurately describing the distribution and volume fraction of a lower-K second phase in the liquid phase sintered BZT-BT, this abbreviated study nonetheless illustrated the utility of the $35Bi_2O_3$-30ZnO-$35B_2O_3$ glass as a sintering aid for 20BZT-80BT. Sintering at 1000°C for four hours yielded dielectrics with useful relative densities (≥93% of the theoretical density of 20BZT-80BT), representing a ≥3% absolute density improvement over 20BZT-80BT sintered under the same conditions. As with the previously studied glass compositions, these liquid phase sintered dielectrics exhibited broad maxima in dielectric constant as a function of temperature with a relatively temperature-stable dielectric constant. The dielectric constant also remained high (>500) at applied electric field strengths of 100kV/cm.

The 1v% $35Bi_2O_3$-30ZnO-$35B_2O_3$ composition shows particular promise for high field, high energy density applications, as the composition reached the highest relative densities of any of the glass compositions and concentrations studied (above 96%) while maintaining high dielectric constant values as a function of field strength and temperature. The energy density of these dielectrics was estimated at 0.5 J/cm^3 at only 100kV/cm field strengths; application of stronger electric fields would, as before, likely increase the energy density to values competitive with polymer film capacitors.

BIBLIOGRAPHY

[1] G.L. Brennecka and H.J. Brown-Shaklee, Sandia National Laboratories (unpublished work).

[2] M.O. Abdullah, *Applied Energy: An Introduction*, CRC Press, Boca Raton, FL, 2012.

[3] A.J. Moulson and J.M. Herbert, *Electroceramics: Materials, Properties, Applications, 2nd Ed.,* John Wiley and Sons, Hoboken, NJ, 2003.

[4] G.A. Samara, "Ferroelectricity Revisited – Advances in Materials and Physics," *Solid State Physics* 56 239-458 (2001).

[5] M.H. Frey, Z. Xu, P. Han, and D.A. Payne, "The Role of Interfaces on an Apparent Grain Size Effect on the Dielectric Properties for Ferroelectric Barium Titanate Ceramics," *Ferroelectrics* 206-207 337 (1998).

[6] L.E. Cross, "Relaxor Ferroelectrics"; pp. 131-155 in Springer Series in Materials Science, Vol. 114, *Piezoelectricity: Evolution and Future of a Technology*. Edited by W. Heywang, K. Lubitz, W. Wersing. Springer Berlin Heidelberg, Berlin, 2008.

[7] T.R. Shrout and J. Fielding, Jr., "Relaxor Ferroelectric Materials," *IEEE 1990 Ultrasonics Symposium* 711-720 (1990).

[8] G.A. Samara, "The Relaxational Properties of Compositionally Disordered ABO_3 Perovskites," *Journal of Physics: Condensed Matter* 15 R367-R411 (2003).

[9] M.R. Suchomel, A.M. Fogg, M. Allix, H. Niu, J.B. Claridge, and M.J. Rosseinsky, "Bi_2ZnTiO_6: A Lead-Free Closed-Shell Polar Perovskite with a Calculated Ionic Polarization of 150 μC cm^{-2}," *Chemistry of Materials* 18 4987-4989 (2006).

[10] A.A. Belik, S. Iikubo, K. Kodama, N. Igawa, S.-I. Shamoto, M. Maie, T. Nagai, Y. Matsui, S.Y. Stefanovich, B.I. Lazoryak, and E. Takayama-Muromachi, "$BiScO_3$: Centrosymmetric $BiMnO_3$-type Oxide," *Journal of the American Chemical Society* 128 706-707 (2006).

[11] A.A. Belik, S.Y. Stefanovich, B.I. Lazoryak, and E. Takayama-Muromachi, "$BiInO_3$: A Polar Oxide with $GdFeO_3$-Type Perovskite Structure," *Chemistry of Materials* 18 1964-1968 (2006).

[12] M.R. Suchomel and P.K. Davies, "Enhanced tetragonality in $(x)PbTiO_3$-$(1-x)Bi(Zn_{1/2}Ti_{1/2})O_3$ and related solid solution systems," *Applied Physics Letters* 86 262905 (2005).

[13] C.-C. Huang and D.P. Cann, "Phase transitions and ferroelectric properties in $BiScO_3$-$Bi(Zn_{1/2}Ti_{1/2})O_3$-$BaTiO_3$ solid solutions," *Journal of Applied Physics* 102 044103 (2007).

[14] S. Wada, K. Yamato, P. Pulpan, N. Kumada, B.-Y. Lee, T. Iijima, C. Moriyoshi, and Y. Kuroiwa, "Piezoelectric properties of high Curie temperature barium titanate-bismuth perovskite-type oxide system ceramics," *Journal of Applied Physics* 108 094114 (2010).

[15] N. Raengthon and D.P. Cann, "High temperature electronic properties of $BaTiO_3$-$Bi(Zn_{1/2}Ti_{1/2})O_3$-$BiInO_3$ for capacitor applications," *Journal of Electroceramics* 28 165-171 (2012).

[16] I. Fujii, K. Nakashima, N. Kumada, and S. Wada, "Structural, dielectric, and piezoelectric properties of $BaTiO_3$-$Bi(Ni_{1/2}Ti_{1/2})O_3$ ceramics," *Journal of the Ceramic Society of Japan* 120 [1] 30-34 (2012).

[17] K. Yamato, N. Kumada, C. Moriyoshi, Y. Kuroiwa, B.-Y. Lee, T. Iijima, and S. Wada, "Crystal Structure Analysis of Barium Titanate-Bismuth Perovskite-type Oxide System Ceramics and Their Piezoelectric Property," *Key Engineering Materials* 421-422 38-41 (2010).

[18] C.-C. Huang and D.P. Cann, "Phase transitions and dielectric properties in $Bi(Zn_{1/2}Ti_{1/2})O_3$-$BaTiO_3$ perovskite solid solutions," *Journal of Applied Physics* 104 024117 (2008).

[19] J.F. Ihlefeld, Ph.D. Dissertation, North Carolina State University, 2006.

[20] I. Barin, *Thermochemical Data of Pure Substances, 3rd Edition*, Weinheim, New York (1995).

[21] D.R. Gaskell, *Introduction to the Thermodynamics of Materials, 5th Ed.,* Taylor and Francis, New York (2008).

[22] M.W. Chase, Jr., C.A. Davies, J.R. Downey, Jr., D.J. Frurip, R.A. McDonald, and A.N. Syverud, *NIST-JANAF Thermochemical Tables, 1985, v 1.0*, NIST, Gaithersburg, MD (1986).

[23] M.N. Rahaman, *Ceramics Processing*, CRC Press, Boca Raton, FL, 2006.

[24] W. Huebner and S.C. Zhang, "High Energy Density Dielectrics for Symmetric Blumleins," *Proceedings of the 2000 12th IEEE International Symposium on Applications of Ferroelectrics* 2 833-836 (2001).

[25] B.-S. Kim, E.-S. Lim, J.-H. Lee, and J.-J. Kim, "Effect of structure change on thermal and dielectric characteristics in low-temperature firing Bi_2O_3-B_2O_3-ZnO glasses," *Journal of Materials Science* 42 4260-4264 (2007).

[26] American Ceramic Society-National Institute of Standards and Technology (ACerS-NIST) Phase Equilibria Diagrams, Diagram #10126-A.

[27] C. Jovalekic, Lj. Atanasoska, V. Petrovic, and M.M. Ristic, " Sintering and characterization of $Bi_4Ti_3O_{12}$ ceramics," *Journal of Materials Science* 26 3553-3564 (1991).

[28] H. Chen, B. Shen, J. Xu, and J. Zhai, "The grain size-dependent electrical properties of $Bi_4Ti_3O_{12}$ piezoelectric ceramics," *Journal of Alloys and Compounds* 551 92-97 (2013).

[29] ACerS-NIST Phase Equilibria Diagrams, Diagram #EC-154.

[30] E.C. Subbarao, "Ferroelectricity in $Bi_4Ti_3O_{12}$ and Its Solid Solutions," *Physical Review* 122 [3] 804-807 (1961).

[31] ACerS-NIST Phase Equilibria Diagrams, Diagram #10341.

[32] K. Uchino and S. Nomura, "Critical Exponents of the Dielectric Constants in Diffused-Phase-Transition Crystals," *Ferroelectrics* 44 [1] 55 (1982).

[33] M. Rabuffi and G. Picci, "Status Quo and Future Prospects for Metallized Polypropylene Energy Storage Capacitors," *IEEE Transactions on Plasma Science* 30 [5] 1939 (2002).

[34] V.K. Seth and W.A. Schulze, "Grain-Oriented Fabrication of Bismuth Titanate Ceramics and Its Electrical Properties," *IEEE Transactions on Ultrasonics, Ferroelectrics, and Frequency Control* 36 [1] 41 (1989).

VITA

David I. Shahin was born in St. Louis, Missouri in 1989 to Issa and Alma Shahin. Throughout his childhood, it became obvious to David and his family that he was destined to be an engineer, due to his love of learning anything related to science and technology, and his tendency to disassemble, tinker with, and repurpose nearly every mechanical or electronic object he could get his hands on. David's time as a student at St. Louis University High School afforded him the opportunity to study and fall in love with chemistry, physics, and calculus.

His passion for math, science, and engineering led David to begin his study of Ceramic Engineering in 2007 at the University of Missouri-Rolla (now Missouri University of Science and Technology) in Rolla, Missouri. David graduated from S&T with his Bachelor of Science degree in Ceramic Engineering in December of 2011. Following completion of his Bachelor of Science studies, David immediately began work towards his Master of Science degree in Ceramic Engineering at S&T, with Drs. Wayne Huebner and Geoff Brennecka as his advisors.

An active participant in student organizations, David was involved in the Materials Science and Engineering Department's Keramos and Material Advantage student chapters; he also learned to blow glass, and was an active member in the S&T Hot Glass Shop and associated student organization, the Gaffers' Guild. David served three years as a delegate and council chair of the American Ceramic Society's President's Council of Student Advisors, was an active member and president of the Catholic Newman Center at S&T, and participated in several co-ops and internships with Sandia National Laboratories.

David will be marrying his fiancé, Katie, in May of 2013. He has chosen to pursue his Ph.D. in Materials Science and Engineering at the University of Maryland-College Park once his M.S. studies are completed.